NAIC-ID(RS)T-0651-94

NATIONAL AIR INTELLIGENCE CENTER

CHINESE SPACE SCIENCE AND TECHNOLOGY
(Selected Articles)

DTIC
ELECTE
JAN 11 1995
B

19950109 112

Approved for public release;
Distribution unlimited.

HUMAN TRANSLATION

NAIC-ID(RS)T-0651-94 13 December 1994

MICROFICHE NR: 94C000551

CHINESE SPACE SCIENCE AND TECHNOLOGY
(Selected Articles)

English pages: 136

Source: Zhongguo Kongjian Kexue Jishu, Vol. 10, Nr. 6, December 1990; pp. I; 1-29; 34-70

Country of origin: China
Translated by: Leo Kanner Associates
F33657-88-D-2188
Requester: NAIC/TASR/Mark Shockey
Approved for public release; Distribution unlimited.

THIS TRANSLATION IS A RENDITION OF THE ORIGINAL FOREIGN TEXT WITHOUT ANY ANALYTICAL OR EDITORIAL COMMENT. STATEMENTS OR THEORIES ADVOCATED OR IMPLIED ARE THOSE OF THE SOURCE AND DO NOT NECESSARILY REFLECT THE POSITION OR OPINION OF THE NATIONAL AIR INTELLIGENCE CENTER.

PREPARED BY:

TRANSLATION SERVICES
NATIONAL AIR INTELLIGENCE CENTER
WPAFB, OHIO

TABLE OF CONTENTS

Accession For
NTIS GRA&I ☑
DTIC TAB ☐
Unannounced ☐
Justification
By
Distribution
Availability Codes
Dist Avail and/or Special
A-1

GRAPHICS DISCLAIMER

All figures, graphics, tables, equations, etc. merged into this translation were extracted from the best quality copy available.

NOT HERE

ABLATIVE THERMAL PROTECTIVE MECHANISM AND NUMERICAL SIMULATION FOR RETURNABLE SATELLITE

Jiang Guiqing of Beijing Institute of Aerodynamics

Abstract: This paper discusses in detail the problem of mass loss and endothermic mechanism for charring material. By using a lamination model, the energy-conservative relations for each layer that has different physicochemical properties are presented. Numerical simulation of thermal protection for each layer is established by the integral method. A comparison with analytical results of one-dimensional heat conduction showed good agreement. The calculated results are also consistent with those from the ablation experiments.

Key words: Ablative material, infinitesimal calculus, reentry vehicle, computation.

I. Foreword

Since the sixties, research and development have been vigorously conducted on returnable satellites and spacecraft in the United States and Soviet Union. As an important integral part (of the development), ablative thermal protection has also been carried out with strenuous efforts in experiments and theoretical research. In the initial state of development, they generally followed the research accomplishments of thermal protection of the reentry terminus of long-range guided missiles; high-density glass-type reinforced plastics were adopted for ablative materials. With enhanced performance of returnable

satellites, design personnel discovered that it is difficult to achieve better thermal protection effect by simply relying on a heat-absorption regime with surface mass loss because surface ablation is very limited owing to the unique features of high enthalpy, low heat current and long duration in the reentry environment of a returnable satellite. As shown by the results of theoretical research of high-speed high-temperature adherent layers, mass ejection at wall surfaces can obviously reduce convective heat flow entering the wall surface; the reduction in efficiency is proportional to h_s/q_{00} (h_s is total enthalpy while q_{00} is convective heat flow with mass ejection). This conclusion inspired designers to use mass ejection of thermally released gas of low-temperature carbonized material to lower the convective heat flow and increase thermal-protective efficiency. Thus, multiple kinds of low-density carbonized material were developed. Table 1 lists several typical thermal-protection systems of returnable spacecraft.

In pursuing the development of returnable satellites in China, research on thermal protection regime and numerical simulation of low-temperature carbonized materials was also conducted. Subsequently, the difference method and integration method were applied to obtain numerical simulation [1] of the thermal response of one-dimensional material with mass ejection, and the chemical reactions in the low-temperature bulk carbonized material. In recent years, finite element numerical simulation [2] of heat conduction on axisymmetric ablative bodies was obtained. Analytical solutions were obtained to all these methods; these solutions were verified from experimental measurements in ground tests and flight tests. Based on detailed analysis of the ablative mechanism of low-temperature carbonized materials in the paper, the integration method is used to present numerical simulation of the thermal response of the bulk material, and surface ablation.

Table 1 Several Typical Thermal Protection Systems in Returnable Spacecraft

参数 / 型号 / 项目	生物卫星	"水星号"载人飞船	"双子星座号"载人飞船	"阿波罗号"载人飞船
执行年份	1959年开始1966年发射1969年毕	1962.2～1963.5	1965.3～1966.11	1966年开始1969年7月登月1972年毕
再入质量 (kg)	223	1 180	2 300	5 470
最大热流kW/m²	1 516	711	477	2 604
平均热流kW/m²	611	272	260	515
差加热量MJ/m²	17.58×10^4	10.59×10^4	14.49×10^4	50.66×10^4
再入时间(s)	348	390	550	980
材料组成	浸渗酚醛—的尼龙布	酚醛—玻璃	酚醛玻璃的蜂窝格内填充硅橡胶 (DC—325)	酚醛玻璃蜂窝格内充填环氧酚醛加石英纤维 (AVCO5029—39)
密度 (原始材料)	1.20	1.73	0.85	0.545
密度 (炭层)	0.304	1.55	0.61	0.288～0.32
原始材料热导系数 W/(m·℃)	0.0024	0.0034	0.0015	0.0012
防热层厚度(mm)	18.3～5.6	16.5	23.4 (平均)	31.5 (平均)

Key: 1. Item; 2. Parameters; 3. Model number; 4. Biological satellite; 5. Mercury manned spacecraft; 6. Gemini manned spacecraft; 7. Apollo manned spacecraft; 8. Year of execution; 9. Reentry mass; 10. Maximum heat flow; 11. Mean heat flow; 12. Difference of heating quantities; 13. Reentry time; 14. Material composition; 15. Density; 16. Original material; 17. Carbon layer; 18. Heat conductive coefficient of original material; 19. Thickness of thermal protective layer; 20. Beginning in 1959, launch in 1966, completion of project in 1969; 21. Beginning in 1966, moon landing in July 1969, completion of project in 1972; 22. Nylon fabric immersed in phenol-aldehyde; 23. Phenol-aldehyde--glass; 24. Silicon rubber filled in honey-comb lattice of phenol-aldehyde--glass; 25. Epoxy phenol-aldehyde and quartz fiber filled in honey-comb lattice of phenol-aldehyde--glass.

II. Ablation Mechanism of Low-Temperature Carbonized Material

Low-temperature carbonized materials can be divided into two categories: low-density and high-density. Low-temperature materials include silicon tiny balls (107 as the code number) filled in a honey-comb lattice of phenol-aldehyde and glass, and phenol-aldehyde tiny balls and quartz fibers (509 as the code number) filled in the honey-comb lattice of phenol-aldehyde--glass. High-density materials include nylon phenol-aldehyde and dacron phenol-aldehyde.

In the ablative process, the low-temperature carbonized materials have the following variations: after heating the material, first there is the thermal dissolution (cracking), which passes through the porous carbon layer to overflow onto the surface of the material. Thus, oxidation (with air oxygen) occurs. After the material thermally dissolves, the remaining portion forms a porous carbon layer. In some materials, the thermally dissolved gas will have secondary thermal cracking when the gas passes through the porous carbon layer. After cracking, the residue remains in the porous carbon layer; this is the so-called carbon deposition. According to the unique features of the physicochemical variations of different portions of the low-temperature carbonized material, three zones can be divided, as shown in Fig. 1.

(A) Zone of original material (this is the zone in the material that thermal cracking does not occur): in this zone, the thermal behavior of the material includes heat conduction and heat absorption (with thermal enthalpy).

(B) Zone of original material (this is also called the thermal cracking zone): this is the zone with the most intensive thermal cracking. The thermal behavior of the material includes thermal cracking of material, flow of thermal-cracking gas, heat conduction and heat absorption with thermal enthalpy.

(C) Carbon layer (this is the zone of residue after the material is thermally cracked): the principal constituent is carbon. The following thermal behavior takes place: gasdynamic heating (including convective heat flow and radiation heat flow)

at surface of carbon layer, heat-blocking effect, re-radiation at material surface, retreating of material surface, combustion reaction of surface carbon, flow of thermally-cracked gas, conduction, carbon deposition and reaction of different phases, such as carbon--silicon reaction.

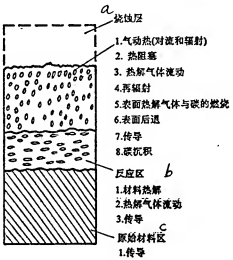

Fig. 1 Ablative mechanism and ablative model of low-temperature carbonized material
Key: (a) Ablation layer: 1. Gas-dynamic heat (convection and radiation); 2. Heat blocking; 3. Flow of thermally cracked gas; 4. Re-radiation; 5. Combustion of thermally cracked gas and carbon at surface; 6. Retreating of surface; 7. Conduction; 8. Carbon deposition; (b) Reaction zone; 1. Thermal cracking of material; 2. Flow of thermally cracked gas; 3. Conduction (c) Zone of original material; 1. Conduction.

Generally, there are primarily the following kinds of mass

loss in the ablative process of low-temperature carbonized material.

(a) Flowing out (and loss) of thermally cracked gas;

(b) Combustion of surface carbon and other chemical erosion; and (c) Mechanical wear of the material.

There are following types of heat absorption regime in ablative process of low-temperature carbonized material:

(1) Thermal cracking of material: after a material is heated, it will crack and absorb heat; the heat absorption quantities are as follows.

For dacron-phenol-aldehyde $\triangle H_p = 231 MJ/kg$

For No. 107 (tiny balls) $\triangle H_p = 124 MJ/kg$

For No. 509 (tiny balls) $\triangle H_p = 87.7 MJ/kg$

For nylon-phenol-aldehyde, it begins to have thermal cracking at 400K; cracking is complete at 800K. There are the following constituents in the thermally cracked gases: H_2, CO, CO_2, CH_4, C_2H_2, C_2H_4, and NH_3, among others.

Table 2 Wearing of Mass from Heating for Several Types of Low-Temperature Carbonized Material

	℃	100	200	300	400	500	600	700	800
1质	509	1.17	5.7	12.7	42.2	54.3	61.2	62	63.5
损	107			5.8	23.6	75.3	78.7	79.5	
%	2酚醛涤纶	1.5	2.5	3.0	10.0	59	66	70	72

Key: 1. Wear of mass; 2. Phenol-aldehyde-dacron.

(2) Flow of thermally-cracked gas: when the gas passes through carbon layer, a portion of heat will be carried away.

(3) Carbonization of material: after a material is thermally cracked, the residue is porous carbon layer, which has the function of blocking heat, thus reducing the amounts of heat conducted to the thermally cracked zone.

(4) Blocking effect of thermally cracked gas: the blocking

effect of gas is the major heat absorption regime of low-temperature carbonized material in the environment of high enthalpy and low heat flow. After passing through the porous carbon layer, the thermally cracked gas escapes from the surface, thus having an ejective function, and reducing convective heat flow.

(5) Combustion of surface carbon: oxidation occurs between surface carbon and air oxygen to release heat.

(6) Surface retreating: due to the combustion of surface carbon, the surface retreats. Owing to surface loosening in some material, mechanical wear can occur, intensifying surface retreat.

(7) Re-radiation: formed at the surface, the carbon layer has a higher radiation coefficient. Hence, radiation from material surface to air is also an important heat-absorbing regime. For example, the radiation coefficient of nylon-phenol-aldehyde is 0.78; the radiation coefficient of No. 509 is 0.6.

(8) Carbon deposition: as indicated in [3], from a chemical analysis and the density profile of the ablation residue of the thermal protection layer on Apollo 1, Apollo 3 and Apollo 4, carbon deposition can be observed. The deposition model can be expressed by the following formula of dynamics.

$$\dot{\rho}\ (\text{deposition}) \doteq A_1(\rho'' - \rho)\exp(-B_1/T)$$

In the equation,

$\dot{\rho}$ (deposition) is the density increase rate of carbon layer caused by deposition;

ρ'' is original density of the material;

ρ is density of carbon layer;

A_1 and B_1 are empirical constants

(9) Heat conduction: this is thermophysical property of conventional materials.

The factors are the conventional properties of the physicochemical variations for low-temperature carbonized materials.

In addition to the above-mentioned properties, organosilicon

107 material has some additional properties as follows.

Following ablation of organosilicon under low heating conditions with heat flow, its surface expands and does not retreat. With the model (ρ 50mm for the original model, and 20mm thickness for the specimen) after ablation in an electric-arc heating device, generally 2 to 3mm of expansion will occur. After ablation of the model, its surface is a layer of a grayish white solid shell (called as carbon layer). The lower layer is the so-called "empty cavity layer" with some powder. Further down below, there is the zone of heat radiation 1 to 2mm in thickness; the next underlying layer is the layer of original material shown in Fig. 2.

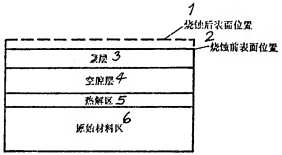

Fig. 2 Ablative layer division of organosilicon 107 material
Key: 1. Position of post-ablation surface; 2. Surface position before ablation; 3. Carbon layer; 4. Empty cavity layer; 5. Heat cracking zone; 6. Zone of original material.

There are following properties in the cracking of organosilicon: produced by one cracking, the volatile cyclosilica alkyl consists of white crystals at room temperature. Owing to differences in silicon molecules, there are crystals with acicular, sheet and snowflake shapes. At high temperatures, these crystals completely sublimate. In 1972, chromatographs were used at the Dalian Institute of Chemistry and Physics to analyze cracked gas constituents. The following constituents were obtained.

(1) At about 1000K, a second cracking occurs in the cyclosilica alkyl, which is the product of the first cracking of the organosilicon.

(2) The cracking products are CH_4, H_2, SiO, SiO_2 and C, among others.

By using the properties of second cracking of organosilicon, some unique structures can be explained after ablation of organosilicon, which commences thermal cracking between 200° and 300°C. The products are volatile cyclosilica alkyl as well as such low-molecule gases as H_2, CH_4, CO, CO_2 and H_2O (among others); these products are released from the main body of organosilicon. Previously added o the material, SiO_2 filler remains. This is the cause of an empty cavity layer forming for some powder. The density of this layer is apparently lower than the original material. When the cyclosilica alkyl diffuses to the surface, second cracking occurs because the surface temperature is higher. The gaseous products (H_2 and CH_4, among others) are released from the surface; however, the solid product SiO_2 remains. Therefore the density of this layer is higher than the density of the empty cavity layer. Since the surface temperature is higher, SiO_2 can be fused. After cooling down, this forms a layer of grayish white firm outer shell. Since an empty cavity layer is formed, this has the following effect: heat-insulating property of organosilicon 107 material is apparently higher than that of epoxyphenol aldehyde 509.

III. Numerical Simulation of Heat Preventive Properties of Low-temperature Carbonized Material

After surface ablation of low-temperature carbonized material during reentry conditions of high enthalpy and low heat flow, its surface retreat is a secondary property; the major property is thermal response in the bulk material.

For convenie ces, the following assumptions are added into derivation and cc utation formulas.

(1) The mate ial is divided into three layers: carbon layer,

thermal cracking layer and layer of original material.

(2) When the thermally cracked gas flows through the carbon layer, the gas does not react with carbon, so secondary cracking does not occur.

(3) It is assumed that the rate of thermal cracking is quasi-steady; there is a relationship of linear function between density and temperature.

Refer to Fig. 1 for division of layers.

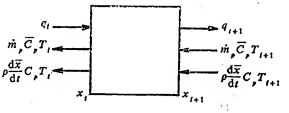

Fig. 3 Single element energy equilibrium of carbon layer

(A) Carbon layer

Carbon layer x is divided into n elements; energy equilibrium is established with i elements.

The rate of heat energy increase for a single element is the energy difference between the inflow and outflow of the element. That is

$$\frac{d}{dt}\int_{x_i}^{x_{i+1}} \rho C_p T dy = q_i - q_{i+1} - \dot{m}_x \widetilde{C}_p (T_i - T_{i+1}) - \rho_i C_{p_i} T_i$$

$$+\rho_{i+1} C_{p_{i+1}} T_{i+1} - \frac{1}{2}\left(\frac{dx_i}{dt} + \frac{dx_{i+1}}{dt}\right)(\rho_i C_{p_i} T_i - \rho_{i+1} C_{p_{i+1}} T_{i+1}) \qquad (1)$$

The trapezoidal formula is adopted for integration at the left-hand side of Eq. (1), and let us assume that density of carbon layer remains unchanged. Thus, we have

$$\frac{d}{dt}(C_{p_i} T_i + C_{p_{i+1}} T_{i+1}) = \frac{q_i - q_{i+1} - \dot{m}_x \bar{C}_p (T_i - T_{i+1}) - \dot{m}_x (C_{p_i} T_i - C_{p_{i+1}} T_{i+1})}{\frac{1}{2}\rho(x/n)}$$

$$-(2i+1)(\rho_i C_{p_i} T_i - \rho_{i+1} C_{p_{i+1}} T_{i+1}) \frac{1}{x} \frac{dx}{dt} \qquad (2)$$

If the variation of specific heat in carbon layer is low, Eq. (2) can be further simplified into

$$\frac{\mathrm{d}}{\mathrm{d}t}(T_i+T_{i+1})=\frac{q_i-q_{i+1}-(\dot{m}_p\overline{C}_p+\dot{m}_cC_p)(T_i-T_{i+1})}{\frac{1}{2}\rho C_p\left(\frac{x}{n}\right)}$$

$$-(2i+1)(T_i-T_{i+1})\frac{1}{x}\frac{\mathrm{d}x}{\mathrm{d}t} \qquad (3)$$

In Eqs. (1), (2) and (3),

$$i=0,\cdots,n-1;\quad x_i=i\frac{x}{n};\quad \dot{m}_c=\rho\frac{\mathrm{d}\bar{x}}{\mathrm{d}t}$$

$$\begin{cases} q_i=\phi q_{00}(1-h_w/h_s)-\varepsilon\delta T_w^4+\dot{m}_s\Delta H_s & i=0 \\ q_i=k\dfrac{(T_{i-1}-T_{i+1})}{2(x/n)} & i\neq 0 \end{cases}$$

(B) Layer of thermal cracking

Divide the thermal cracking layer x' into m equal parts; establish energy equilibrium on j elements (refer to Fig. 4).

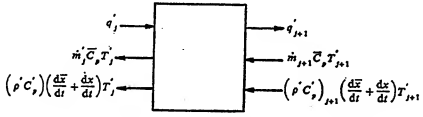

Fig. 4 Energy equilibrium of element in thermal cracking layer

In contrast to the carbon layer, density variation is intensified with heat absorption from thermal cracking in this thermal cracking layer. Hence, energy conservation of j elements is

$$\frac{\mathrm{d}}{\mathrm{d}t}\int_{x_j}^{x'_{j+1}}\rho'C'_pT'\,\mathrm{d}y-\int_{x_j}^{x'_{j+1}}\dot{w}_p\Delta H_p\,\mathrm{d}y=q'_j-q_{j+1}-(\dot{m}'_j\overline{C}_pT'_j-\dot{m}'_{(j+1)}\overline{C}_pT'_{j+1})$$

$$-\left(\frac{\mathrm{d}\bar{x}}{\mathrm{d}t}+\frac{\mathrm{d}x}{\mathrm{d}t}\right)[(\rho'C'_pT')_j-(\rho'C'_pT')_{j+1}]+\frac{1}{2}\left(\frac{\mathrm{d}x'_j}{\mathrm{d}t}+\frac{\mathrm{d}x'_{j+1}}{\mathrm{d}t}\right)[(\rho'C'_pT')_j,$$

$$-(\rho'C'_pT')_{j+1}] \qquad (4)$$

The second term on the left-hand side of Eq. (4) is thermal

cracking heat absorption of the material.

In the equation, $\dot{w}_\rho$ is the rate of thermal cracking

$$m_{\rho j}' = \int_{x_j'}^{x_{j+1}'} \dot{w}_\rho \mathrm{d}y = \frac{\mathrm{d}\rho'}{\mathrm{d}T'} \int_{x'}^{x'_{i+1}} \frac{\partial T'}{\partial t} \mathrm{d}y,$$

$$x_j' = j\frac{x'}{m}.$$

The trapezoidal formula is used for integration of the left-hand side of Eq. (4). After manipulation, it becomes

$$\begin{aligned}
&\frac{\mathrm{d}}{\mathrm{d}t}[(\rho' C_\rho' T')_j + (\rho' C_\rho' T')_{j+1}] \\
&= \frac{(q_j' - q_{j+1}') - [m_{\rho,j}'(\overline{C}_\rho T_j' + \Delta H_\rho) - m_{\rho,(j+1)}'(\overline{C}_\rho T'_{j+1} + \Delta H_\rho)]}{\frac{x'}{2m}} \\
&- \frac{[(\rho' C_\rho' T')_j - (\rho' C_\rho' T')_{j+1}]\left(\frac{\mathrm{d}\bar{x}}{\mathrm{d}t} + \frac{\mathrm{d}x'}{\mathrm{d}t}\right)}{\frac{x'}{2m}} \\
&- (2j+1)[(\rho' C_\rho' T')_j - (\rho' C_\rho' T')_{j+1}]\frac{1}{x'}\frac{\mathrm{d}x'}{\mathrm{d}t} \qquad (5)
\end{aligned}$$

In the equation,

$$j = 1, \cdots, m-1, \quad q_j' = k'\frac{(T'_{j-1} - T'_{j+1})}{2(x'/m)}.$$

$m_{\rho j}'$ is determined by the continuous equation

$$\begin{aligned}
m_{\rho,j}' &= m_{\rho,(j+1)}' - \int_{x_j'}^{x'_{j+1}} \frac{\partial \rho'}{\partial t} \mathrm{d}t \\
&= m_{\rho,(j+1)}' - \left(\frac{\mathrm{d}\rho'}{\mathrm{d}T'}\right)\left[\frac{x'}{2m}\left(\frac{\mathrm{d}T_j'}{\mathrm{d}t} + \frac{\mathrm{d}T'_{j+1}}{\mathrm{d}t}\right) - \left(\frac{j+1}{m}T'_{j+1} - \frac{j}{m}T_j'\right)\frac{\mathrm{d}x'}{\mathrm{d}t}\right]
\end{aligned}$$

$$m_{\rho 1}' = m_{\rho 1}.$$

(C) Layer of original material

In this layer, the physicochemical properties of the material remain unchanged. Divide x" into S equal parts. For the same reason, we have

$$\frac{\mathrm{d}}{\mathrm{d}t}(T_i'' + T''_{i+1}) = \frac{q_i'' - q''_{i+1}}{\frac{1}{2}\rho'' C_\rho''(x''/s)} - (2s-2k-1)\frac{1}{x''}\frac{\mathrm{d}(\bar{x} + x + x')}{\mathrm{d}t}(T_i'' - T''_{i+1}) \qquad (6)$$

In the equation, $k = 1, \cdots, s-1$; $q_i'' = \frac{k''(T''_{i-1} - T''_{i+1})}{2(x''/s)}$.

The initial and boundary conditions are given in the following.

The initial condition: $t=0 \quad T(y,0)=300\text{K}$

The surface condition: $y=\bar{x}$

$$-k\frac{\partial T}{\partial y}=\phi q_{c0}(1-h_w/h_s)-\varepsilon\sigma T_s^4+\dot{m}_c\Delta H_s$$

Conditions at the boundary surface:

$y=\bar{x}+x$

$T_s=T'_s=T'\text{II} \quad q_s=q'_0$

$y=\bar{x}+x+x'$

$T''_s=T'_s=T\text{I} \quad q'_w=q''_0$

$y=\bar{x}+x+x'+x''$

adiabatic material or compatible with heat-insulating material.

In the above-mentioned conditions, T_I is temperature at beginning of thermal cracking; T_{II} is the temperature at the end of thermal cracking.

Supplementary relation equations:

$$\phi=1-0.724(\dot{m}_c+\dot{m}_p)h_s/q_{c0}+0.13(\dot{m}_c+\dot{m}_p)^2h_f^2/q_{c0}^2$$

$$\dot{m}_c=\frac{\widetilde{C}_{O_2c}/(1+B)}{\dfrac{1}{\overline{a}_{ch}}+\dfrac{1}{a_{d1}}} \qquad T_w<1\,700\text{K}$$

$$\dot{m}_c=0.1725\phi q_{c0}/h_s \qquad T_w>1\,700\text{K}$$

$$a_{d1}=\frac{M_c}{M_s}(1+B)\phi q_{c0}/h_s$$

$$\overline{a}_{ch}=\frac{a_{ch}(1+B)^{1/2}}{(\widetilde{C}_{O_2c}-\dfrac{M_c}{M_s}B_s)^{1/2}}$$

$$a_{ch}=k_0e^{-E/RT_w}\left(\frac{\overline{M}}{M_{O_2}}P_s\right)^{1/2}$$

$$B=B_s+B_p$$

$$B_s=\frac{\dot{m}_c}{(\phi q_{c0}/h_s)} \qquad B_p=\frac{\dot{m}_p}{(\phi q_{c0}/h_s)}$$

If the thermal-cracking zone is simplified into thermal cracking, the rate of mass loss in thermal-cracked gas is

determined by the following equation of mass equilibrium.

$$\dot{m}_r = (\rho'' - \rho)\left(\frac{\mathrm{d}\bar{x}}{\mathrm{d}t} + \frac{\mathrm{d}x}{\mathrm{d}t}\right)$$

In the above equation, ρ" and ρ are the densities of original material and carbon layer, respectively.

IV. Calculated Examples

Three calculated examples are given below. The first and second examples are used to verify the correctness of the computational method; the third example is to present the influence of calculated results on the model of the thermal-cracking surface by the thermal-cracking zone.

(A) Comparison between computational method and results of analytical solution in the paper

Assume that there is a level plate with thickness L. One end of the plate contacts the heat source while the other end is adiabatic. The analytical solution is

$$T = T_f\left\{1 - 2\sum_{i=1}^{\infty}\frac{\sin\mu_i L\cos\mu_i L}{\mu_i L + \sin\mu_i L\cos\mu_i L}\exp(-\mu_i^2\frac{\kappa}{\rho C_p}\tau)\right\}$$

In the equation, μ_i is the solution of equation $\tan\mu_i L = \frac{\mathrm{d}L}{\kappa}\frac{1}{\mu_i L}$;

α is the heat transfer coefficient; and

κ, ρ, C_p is the corresponding heat-conductibn coefficient, density and specific heat.

Table 3 Comparison Between Method in This Paper and Analytical Solution

方 法 a	t=0	t=10	t=20	t=30	t=50	t=70
解 析 解 b	0.00000	0.38431	0.47684	0.53284	0.60264	0.64685
本文方法 c	0.00000	0.38876	0.47675	0.53286	0.60272	0.64694

Key: a. Method; b. Analytic solution; c. Method in this paper

(B) Comparison of results between the method given in this paper, and ground experiments

Table 4 presents a comparison between the experimental results (of ablation and temperature measurement of the electric-arc heating device) and calculated results using the method presented in the paper. The material parameters of the physical properties in the experimental model are given in the appendix.

Table 4 Comparison of Calculations in the Paper and Results of Ground Experiments

a 状态	h_t MJ/kg	q_{cs} KW/m²	p_t Mpa	t s	x'_0 mm	实验结果 b ΔT_0(K)	ΔT_3(K)	ΔT_5(K)	计算结果 c ΔT_0(K)	ΔT_3(K)	ΔT_5(K)
1	16.33	879 2	0.087	72	15	6～12	86～99	96～106	1.2	97.4	112.7
2	18.84	248 7	0.025	67	25	0～2	7.5～12	22.5～25	0	9.7	31.4
3	17.58	121 4	0.074	48	15	0	62～75	80～90	0	66.2	84
4	10.05	138 2	0.10	120	25	1	26～34	49～65	0.1	36.9	69.1

Key: a. State; b. Experimental results; c. Calculated results.

In Table 4, x'_0 is thickness of model; ΔT_0 is temperature increase at the rear of the model when heating is terminated; ΔT_3 is temperature increase at the rear 3min after heating is terminated; ΔT_5 is temperature increase at the rear 5min after heating is terminated.

(C) Comparison between calculated results of thermal-cracking zone model, and thermal-cracking surface model

The amount of calculations is large for the model of the thermal-cracking zone. To satisfy requirements of engineering calculations, generally we use thermal-cracking surface to represent the thermal-cracking zone. Their differences can be shown in Table 5, which gives the calculated results for two ground experimental states.

Table 5 Comparison of Calculated Results Between Models of Thermal-cracking Zone and Thermal-cracking Surface

状态[a]	$\bar{x}$ (mm)	x (mm)	x' (mm)	ΔT_s (K)	备注[d]
1	0.4525	4.266	1.825	21.0	热解区模型[b]
	0.4229	4.625		15.7	热解面模型[c]
2	0.3254	3.834	2.526	141	热解区模型[b]
	0.2745	4.511		111.4	热解面模型[c]

Note: in the table, $\bar{x}$ is ablation thickness; x is thickness of carbon layer; x' is thickness of thermal-cracking layer.
Key: a. State; b. Model of thermal cracking zone; c. Model of thermal cracking surface; d. Remarks.

The temperature at the rear of the model of the thermal-cracking surface is lower than for the model of the thermal-cracking zone; however, the difference is small. Hence, the model of the thermal-cracking surface can be used for the initial estimate.

V. Conclusions

The paper analyzes in detail low-temperature carbonized material. By using models of layer division, the equations of energy equilibrium are established for various layers; the integration method is used in the numerical simulation of thermal protection of low-temperature carbonized material. As shown in calculations of several examples, the calculated results in the paper are consistent with the results from the analytical solution. As shown in the calculation of the ablative experimental state with the electric-arc heating device, the calculated results in the paper are in quite good agreement with ground experimental results. This proves that the calculation method presented in the paper can satisfy the requirements of engineering calculation. It further reveals in the calculated examples the difference is minor between the calculated results of thermal-cracking surface model, and the results of the thermal-cracking zone model. As an initial estimate, it is

suggested that calculations be made with the thermal-cracking surface model.

APPENDIX

The following physical parameters and other constants of material can be used in calculation:

Original material, $T<573\text{K}$

$$\rho''=1300\text{kg/m}^3$$
$$C_p''=1\ 507\text{J/(kg·K)}$$
$$\kappa''=2.407\times10^{-1}\text{W/(m·K)}$$

Thermal-cracking layer,

$573\text{K}<T<873\text{K}$

$$\rho'=1300-2.979\ (T'-573)\quad(\text{kg/m}^3)$$
$$C_p'=4187\times[0.36+0.1017\times10^{-3}(T'-573)]\text{J/(kg·K)})$$
$$\kappa'=4187\times[0.575\times10^{-4}+0.4730\times10^{-6}\ (T'-573)\ ]\ (\text{W/(m·K)})$$

Carbon layer,

$T>873\text{K}$

$$\rho=406.3\text{kg/m}^3$$
$$C_p=4187\times[0.2183\times T/1000+161]\text{J/(kg·K)}\qquad 873\text{K}<T<1\ 973\text{K}$$
$$C_p=2\ 345\quad\text{J/(kg·K)}\qquad T>1\ 973\text{K}$$
$$\kappa=\rho C_p\cdot4187\times\left[0.018\frac{T}{1000}-0.0069\right]\times10^{-4}\quad\text{W/(m·K)}$$
$$T_{\text{I}}=573\text{K}\qquad T_{\text{II}}=873\text{K}$$
$$\Delta H_p=231\ 541\ \text{J/kg}\qquad \varepsilon=0.85$$

Other constants,

$$\bar{C}_p=3\ 266\ \text{J/(kg·K)}\qquad \Delta H_c=9\ 580\times10^3\ \text{J/(kg·K)}$$
$$E/R=21.3\times10^3\ (\text{K})$$
$$k_0=6.89\times10^8\ \text{kg/m}^2\text{s (MPa)}^{1/2}\qquad M=29$$

The paper was received for publication on 4 April 1990.

REFERENCES

1 Jiang Guiqing, AIAA,79—1056

2. Cao Shusheng, Tong Binggang, Jiang Guiqing and Wang Shuhua, "Finite Element Calculations of Heat Conduction in Axisymmetric Ablative Body," Collected Papers of the Fourth All-China Computational Fluid Society, 1988.

ry Denald M an—5969

ABLATIVE THERMAL PROTECTION STRUCTURE DESIGN OF BALLISTIC RETURN MODULE

Chen Qinghua of Beijing Institute of Spacecraft Systems Engineering

Abstract: The paper presents ablative thermal protection structure design of a ballistic return module of satellite. Concepts, material selection, design approach and analytical computations are given. Finally, evaluation of this thermal protection structure is made.

Subject Terms: Thermal protection structure, Ablative material, Ballistic reentry vehicle, and Design.

I. Foreword

There are three following types of thermal protection structure of return module of a ballistic reentry spacecraft: ablative thermal protection structure, radiation thermal protection structure, and heat absorption type thermal protection structure. On deciding which of the above-mentioned thermal structures to be adopted, the choice should be made on the peak heat current density during reentry, and the total heat addition during the reentry process.

Within the range of heat current density (4.2×10^5 to 4.2×10^7 W/m^2) and the total heat addition (4.2×10^5 to 4.2×10^8 J/m^2), the ablative thermal protection structure should be adopted. Moreover, the structure is extensively used on successful flight spacecraft [1, 2].

The return module should pass through three stages of heating environment: heating environment of the ascent stage, orbital stage and return stage. Design with respect to thermal performance should be based on the heat environment in the return stage while design with respect to structural coordination performance should be based on thermal environment in the orbital stage.

II. Selection of Ablative Thermal Protection Structure Scheme and Materials

(A) Design route of ablative thermal protection structure

There are two design pathways in ablative thermal protection structure: whole depth ablation and partial depth ablation as shown in Fig. 1. [3]

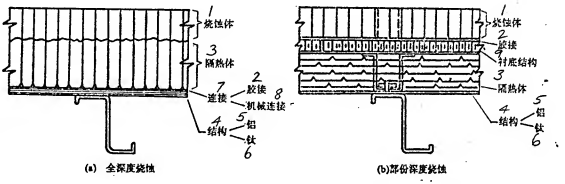

Fig. 1 Two Design Pathways of Ablative Thermal Protection Structure
Legend: (a) Whole depth ablation; (b) Partial depth ablation
Key: 1. Ablative body; 2. Gluing; 3. Heat insulation body; 4. Structure; 5. Aluminum; 6. titanium; 7. Connection; 8. Mechanical connection; 9. Lining structure.

In the case of partial depth ablation in the system design of the thermal protection structure, adiabatic materials whose

heat insulation property is better than the ablative material are used to replace that portion of the ablative material with heat insulation function; thus, the thermal efficiency of the entire thermal protection structure is apparently increased. Comparing both design schemes, the structure is more complex in the latter design, with more factors considered in material selection; thus, it is more difficult technically in design. Between the ablative material layer and the heat insulation layer (use of metallic honeycomb or nonmetallic honeycomb), the adhesive material should be a high-temperature adhesive. During structural design and material selection, sufficient consideration should be given to the structural coordination problem of the three layers (ablative layer, heat-insulating-material layer and force-acting-structural layer).

Fig. 2 shows the structure layout of the whole depth ablation thermal protection structure used in return modules. The temperatures at the adhering surface are relatively low therefore conventional adhesive can be used since it operates at relatively low temperatures. Since the ablative layer directly adheres to the force-acting structure, the overall property between the ablative layer and the force-acting structure is upgraded. The system is easy to be technically realized because of simple structure and high reliability.

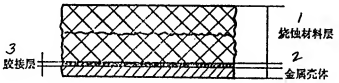

Fig. 2. Ablative thermal protection structure of return module
Key: 1. Ablative material layer; 2. Metallic shell; 3. Adhering layer.

(B) Selection principle of ablative materials

There are relatively many kinds of ablative materials. During the reentry process of the return module, there are the following features of thermal environment: high enthalpy, low pressure, low peak value of heat current density, long reentry duration, and high heat load. These factors require good ablative properties in the ablative material; in addition, the material should have good heat insulation property. By analyzing the ablation regime of several kinds of ablative materials, and through numerous experiments and studies, the result reveals that the most effective ablative material for the return module is an ablative material with low temperature dissolution and carbonization. This kind of ablative material has the following properties.

(1) Good effect on evaporation and cooling: heat is absorbed during heating process of low-temperature carbonization of ablative material; large amounts of gases are released during material dissolution, forming a carbon layer on the surface. Through the carbon layer, the dissolved gas is emitted and enters the adhesive-surface layer, thus generating a heat blocking effect. The greater the amount of the emitted gas, the greater the gas-dynamic heat quantity with a reduction in the blocking effect. The gasification fractions of ablative material with low-temperature dissolution and carburization are relatively high. The gasification fraction can be as high as 70 percent for phenol-aldehyde-nylon composite material, a typical low-temperature carbonized ablative material.

(2) After ablation of low-temperature carbonized ablative material, the carbonization layer formed is generally composed of carbon, which has a high radiation coefficient. At high temperatures, the material can re-radiate large amounts of heat. Fig. 3 shows a distribution diagram of heat quantity during ablation of this kind ablative material[4].

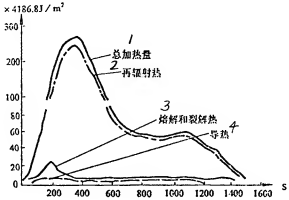

Fig. 3 Distribution of heat quantity during ablation for low-temperature carbonized ablative material
Key: 1. Total heat applied; 2. Re-radiated heat; 3. Fusion and cracking heat; 4. Conductive heat.

(C) Selection method of thermal properties of ablative materials

The heat-quantity density is low over a single area of surface on the return module during reentry, but the total heat quantity added is high. This requires that the ablative material not only have good ablative properties, but also good heat-insulating properties. In indicating the heat-insulating properties of a material, its comprehensive parameter is the ratio $\rho \cdot k/c_p$. The lower the ratio, the better is the heat-insulating property of the material. The lower the material density ρ and the heat-conduction coefficient k, and the higher the specific heat capacity c_p, the lower is $\rho \cdot k/c_p$. From the above-mentioned analysis, we know that the most ideal ablative material for a return module is low-temperature carbonized ablative material with low density.

III. Structural Coordination Property of Ablative Thermal Protection Structure [5, 6]

Since a return module operates in orbital space for a relatively long period, selection of ablative material should be focused on the following points: good ablative properties and heat insulating properties, vacuum radiation-resistant property in space, yieldability between the material and the force-acting structure, and formability of the material, among others.

In selecting thermal protection materials for a return module, structural coordination of the material is a relatively striking problem. Although some materials have very good thermal properties, yet the structural coordination property is undesirable (in other words, there is a relatively large difference between the linear expansion coefficient of the material, and that of the force-acting structure), the material and the structure are not compatible during heating and cooling.

(A) Damage caused by structural mismatch

Owing to structural mismatch, the ablative thermal prevention structure may damage the thermal protection structure.

(1) In a cool environment, there is tensile damage to the ablative layer, and compressive damage to the metallic structure.

(2) There is compressive damage to the ablative layer during the return process.

(3) In a cool environment, there is tensile damage to the adhesive layer, or shearing damage of the edges.

In a general situation, the strength of resin composite materials is lower than that of metallic material; in particular, the tensile strength of plastics is relatively poor. When the return module is in the low-temperature environment of the orbital stage, the ablative layer is in the tensile state as it is in compression along the structure because linear expansions are inconsistent between the ablative layer and the structural layer (in the general situation, the linear expansion coefficient of plastics is greater than that of metals). Therefore, it

appears relatively striking in preventing tensile damage to the ablative layer at low temperatures.

(B) Measures to solve the problem of structural mismatch

There are three technical routes to solve the problem of coordination between the material layer and the structure.

(1) Select such ablative materials with linear expansion coefficients that approximate that of the structure, or select such ablative materials with better elasticity; thus, the stress induced by expansion mismatch can be reduced.

(2) Improve connection mode between the ablative thermal protection layer and the structure layer; or change the structure of the thermal protection system.

(3) Adhesives of better flexibility are selected between the ablative layer and the structural layer; thus, the adhesive layer has sufficient elasticity and strength with a greater temperature range. This can adjust the strain (induced by different thermal expansions) between the structure and the ablative thermal protection layer. This kind of compressive flexible adhesive system can absorb large amounts of deformation energy due to shearing, compression and tension, thus compensating for the inconsistent thermal expansions between the ablative thermal protection layer and the structural layer.

IV. Thermal Analysis of Ablative Thermal Protection Structure [3, 7, 8]

When selecting the thermal protection regime and the design of thermal protection structure, a thermal analysis should be made of the ablative thermal protection structure based on the thermal environment; the following determinations should be made: kind of ablative material, thickness of ablative layer, thickness of adhesive layer, operating temperatures of adhesive layer and force-acting structure, as well as temperature distribution at various sites along the direction of layer depth.

(A) Criterion of thermal design on ablative thermal protection layer

Thickness of the ablative thermal protection layer is determined by the following factors.

(1) The design condition is so selected that the exterior heat flow in the heating ballistic will release the maximum total heating quantity possibly appearing in the reentry corridor.

(2) The allowable use temperature between the ablative thermal protection layer and the heat insulating layer (or the force-acting structure layer) is an important factor.

(3) The allowable operating humidity of the material at the force-acting structure layer is also a factor.

(4) If the entire module adopts a design of equal thickness, the maximum heat-load site should be picked as the cross section for making the thermal analysis. If a design of variable thickness is adopted for the whole module, various sites with unique representation feature should be chosen for the thermal analysis.

(B) Comparative selection of ablation computational model

Heating of exterior heat current produces three zones in the low-temperature carbonized ablative material: carbonization zone, reaction zone (dissolving zone) and primitive material zone, referring to Fig. 4(a).

Based on the features of three zones, an equation of heat conduction medium is established; with known boundary conditions and initial conditions, the thermal analytical computations can be carried out. For simpler computations, the reaction zone can be compressed into a surface as shown in an ablative model in Fig. 4 (b).

With respect to the thermal protection structure of return module, the thermal analysis is computed by using two ablative models. In addition, the computational results are compared with ground test and flight test results. In the case of the extent by which the carbon layer surface has retreated, fundamental

consistency is obtained by comparing the computational results and the results of testing the two ablative models. In the case of carbon-layer thickness and temperature distribution along the depth direction of the ablative thermal protection structure, the results are relatively consistent between the computational results and the test results by using the ablative model as shown in Fig. 4 (a). The carbon-layer thickness computed by using the ablative model in Fig. 4 (b) is somewhat thicker as compared to the experimental value; the computational results are lower for the surface temperature, and higher for the temperature at the back wall.

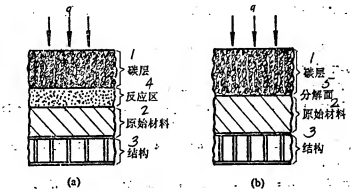

Fig. 4 Two models of ablation computation
Key: 1. Carbon layer; 2. Original material; 3. Structure; 4. Reaction zone; 5. Dissolving surface.

The computation model in Fig. 4 (a) should be adopted in design computations of heat analysis on the ablative thermal protection structure of return module. If the computational model in Fig. 4 (b) is used in design computations, the design will be on the conservative side; however, the computational model can be used in making general estimates.

V. Results

The ablative thermal protection structure is a thermal protection structure with relatively widespread application in thermal protection of reentry modules. This ablative structure serves in single use only in the return module of returnable satellite, and reentry spacecraft.

The ablative thermal protection structure has relatively high capability of adapting to variations in exterior heat flows. This is because the variation of heat flow density is not sensitive for ablative materials; a variation of local site or the instantaneous heat-flow density cannot cause damage to the thermal protection structure. Conversely, the heat efficiency of the thermal protection structure will increase with increasing heat-current density within a certain range; therefore, this is a thermal protection structure with relatively high reliability.

In designing the ablative thermal protection structure, consideration is first given to the heat-flow density and to the heating quantities in the reentry orbit; sufficient consideration is also given to heat coordination between the thermal protection layer and the structural layer in the alternately changing environment of high and low temperatures in the operating orbit.

Consideration should also be given to the capability of ablative materials to withstand vacuum, radiation and low-temperature immersion when selecting materials. Finally, the decisive factor of a thermal protection structure is its feasibility.

The paper was received for publication on 30 March 1990.

REFERENCES

1 Bryan Erb R, Greenshields D H, Chauvin L T and Pavlosky J E. Apollo Thermal-protection System Development. AIAA. paper No68-1142

2 Pavlosky J E and Ieslie G st Leger. Apollo Experience Report-Thermal protection Subsystem. NASA. TND-7564.1974.

3 Mecown James W. Review of Structural and Heat-Shield Concepts for Future Re-Entry. AIAA. Paper No68-1127.1968.

4 Kotanchik J M. Manned Spacecraft Materials Problems. Astronautics/Aeronautics. 1964, 2 (7) : 12~17

5 Vaughan W L. Elastomeric Adhesives for Aerospace Applications. 7 th Annual SAMPE National Symposium Trausaction. 9-1-9-26, 1964.

6 Kuno James K. Compassion of Adhesive Classes for Structural Bonding at Ultrahigh and Cryogenic Temperature Extremes. 7 th Annual SAMPE National Symposium Trausaction. 12-1, 1964.

7 Curry D M. An Analgsis of a Charring Ablation Thermal Protection System. NASA. TND-3150.1965.

8 Swann Robert T, Pittmen, Cland M. Numerical Analysis of the Transient Response of Advanced Thermal Protection Systems for Atmospheric Entry. NASA TND-1370. 1962.

THERMAL CONTROL DESIGN OF RETURNABLE SATELLITE

Xu Jiwan of Beijing Institute of Spacecraft Systems Engineering

Abstract: This paper presents the thermal control subsystem of a Chinese returnable satellite. According to satellite characteristics, the thermal inertia method used in thermal design is described. The temperatures obtained from orbit telemetry data agree with the ground tests. The thermal control subsystem satisfactory provided the temperatures of the structure and the equipment met the design requirements.

Key words: Recoverable satellite, temperature control, thermodynamic test, thermal analysis, design.

I. Foreword

As to the purpose and contents of thermal design of returnable satellites, a beneficial thermal environment is provided for instruments and equipment in the satellite (by adopting various thermal control measures) to allow them to operate normally and within the optimal range of environment temperature for their performance.

Generally, there are three fundamental directions for satellite thermal design.

(1) The satellite is subjected to research and analysis for the potentially encountered heat sources, heat sinks and channels of heat transfer while it is in orbit. Thus, a thermal mathematical model can be established for thermal analysis.

(2) By appropriate thermal control measures, maintain the instruments and equipment in the satellite at the temperature level and within the temperature range.

(3) Experimental verification is conducted in ground thermal experiments.

For China's returnable satellites, its exterior is a nose cone; the satellite is divided into two major portions: return module and instrumentation module. Within the return module, instruments are installed on an H-beam. The instrumentation module is further divided into a transitional compartment and a sealed compartment, within which the instruments are installed on a main beam.

The major features of thermal control design of returnable satellites are as follows.

(1) There is no fairing outside the satellite. In the ascent flight stage, the satellite exterior surface is in an environment of relatively severe gas dynamic heating and gas-current impulses.

(2) The satellite operates in a near-earth orbit with a short orbital period. When in an orbit with the greatest shadow, the satellite's shadow zone occupies a high ratio in the entire orbit, as much as 41 percent. Moreover, the earth's albedo and its infrared radiation account for a high external heat flow ratio in space as received by the satellite.

(3) The satellite operates for a short period of time in orbit.

(4) The three satellite axes are maintained steady; one face of the satellite is continually directed toward the earth.

(5) The satellite structure is complex while its heat capacity is relatively high.

(6) In orbit, there is a gas-filled state in the satellite's sealed compartment.

(7) The satellite power supply consists of chemical batteries.

(8) Most instruments and equipment in the satellite have

relatively high requirements as to environmental temperature.

From these features, the thermal control design of a returnable satellite adopts a scheme mainly of passive thermal control. A schematic diagram of thermal control structure is shown in Fig. 1.

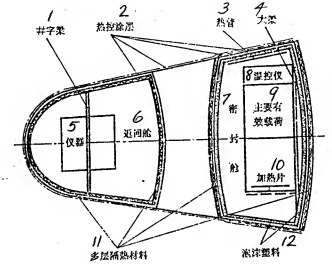

Fig. 1. Thermal control structure of returnable satellite
Key: 1. H-beam; 2. Thermal control coating layer; 3. Heat pipe; 4. Large beam; 5. Instruments; 6. Return module; 7. Sealed compartment; 8. Thermal control instrument; 9. Major payload; 10. Heating plates; 11. Multi-layer heat-insulating material; 12. Expanded plastic

II. Schemes of Thermal Analysis and Thermal Control

In the thermal analysis of the returnable satellite, the first step is the establishment of a thermal mathematical model. According to the overall layout, structure, orbit and attitude parameters, and thermal properties of various portions of the satellite, it is divided into several isothermal nodal points as a simplified mathematical model in thermal analysis and computation.

Based on mission requirements, the attitude of the returnable satellite is three-axis stabilization, orientation toward the earth, large variation of i_0 (the included angle between the operating orbital plane and the sunlight that the satellite possibly confronts), and a relatively large variation of the sunlight factor (τ_s/τ_0=0.59 to 0.75), therefore, for different operating orbits, there is a greater difference in heat flow arriving at the satellite surface. For orbits with maximum shadow, the sunlight factor (τ_s/τ_0=0.59), at that time the orbital plane is nearly parallel with sunlight. Within the same period, there are widely different space heat flows received by different portions and at different time (for the same portion) of the satellite. For an orbit with the sunlight factor (τ_s/τ_0=0.75), half the satellite is always in sunlight in the sunlit zone, while the other half is always out of sunlight. Thus, there is a great difference in heat flow between the surface in sunlight and the other surface in the shade.

Under different orbital conditions, to understand the space heat flow received by different portions of the satellite, and the temperature distribution on the satellite surface, several isothermal nodal points are divided along the circumference direction and according to modules and compartments on the conical surface of the satellite, they are divided into several isothermal nodal points; with the addition of isothermal nodal points on the nose cone and the sealed bottom, they are divided into more than 100 isothermal nodal points for the entire satellite. The energy equilibrium equation of isothermal nodal points is

$$Q_{ss}+Q_i+Q_c+GC_r\frac{dT}{d\tau}=\sigma\varepsilon\overline{T}^4 \qquad (1)$$

In the equation,

Q_{SS} is the summation of solar radiation, earth reflection and earth's radiation heat flow as absorbed by the surface of the isothermal nodal points;

Q_i is heat liberating power inside isothermal nodal points;

Q_c is heat transfer among isothermal nodal points;

G is mass of isothermal nodal points;

C_p is mean specific heat of isothermal nodal points;

$dT/d\tau$ is mean temperature variation rate of isothermal nodal points;

σ is Stefan-Boltzmann constant;

$\bar{\varepsilon}$ is the mean infrared emission rate at surface of isothermal nodal points;

T is mean temperature on surface of isothermal nodal points.

Based on the results of thermal analysis and computation, the satellite thermal control system arrangement is determined as follows: the entire satellite applies passive thermal control as the foundation; active thermal control is supplementary for instruments and equipment with special requirements. The explanation is given below.

(A) Return module

Since the compartment walls are under intensive gas-dynamic heating, a nonmetal thick-wall ablative material is adopted for the compartment wall structure. When the satellite operates in an orbit with a sunlight factor $\tau_s/\tau_0=0.75$, severe deformation (even breaking up) of the satellite structure may occur in the structure of certain ablative material because of high temperatures at the sunlit surface, and low temperatures in the shady surface. To reduce the circumference-direction temperature difference at the satellite surface, it is required to adopt a coating layer on sunlit surface with a low ratio between the solar absorption rate α_s and the infrared emission rate ε_H. However, since the heat liberating power inside the return module is only 9W, it is required to adopt a coating layer with relatively high absorption to radiation ratio ($\alpha_s/\varepsilon_H=1.0$) as in the orbit of maximum shade with the sunlight factor $\tau_s/\tau_0=0.59$ in order to maintain the temperature environment higher than 0^0C inside the compartment, and it is also required to raise the mean

temperature on the interior compartment surface. Moreover, to reduce the range of fluctuations in the surface temperature between the sunlit zone and the shadow zone while in orbit, it is required to have a coating layer with a low infrared emission rate (ε_H). Based on the optimal compromise result of thermal computations, when the maximum sunlight factor is τ_s/τ_0=0.75 in the operating state, a coating layer of slightly lower ratio between absorption and radiation (α_s/ε_H=1.0) is adopted on the sunlit surface (that part of satellite in direct sunlight) occupying 3/20-ths of the circumferential-direction area, and this coating layer is with slightly higher ratio between absorption and radiation (α_s/ε_H=1.2) on the other surface area. For both coating layers, their infrared emission rates are similar, ε_H=0.5. As indicated in the thermal analysis, this thermal design can satisfy requirements of temperature differences on compartment walls, and the temperature environment of instruments and equipment inside the compartment either under operating conditions of high temperatures in orbit at the maximum sunlight factor, and low temperatures in orbit in maximum shade. In the thermal design of the return module, consideration is given to the high-temperature operating conditions of the maximum sunlight factor, the temperature difference is relatively high in the compartment nearing the sunlit surface, and the other compartment portion nearing the shadow surface; thus, the temperature difference among instruments is relatively high, not easily meeting the temperature requirements of instruments. Hence, the multi-layer heat insulation material is laid out on the return module interior walls, thus equalizing the circumferential-direction temperature inside the module. After taking this approach, temperature rises in the instruments inside the module can also be controlled during satellite reentry. Again, based on the property of low heat liberating power inside the return module, in order to maintain temperature level inside the module at the maximum shade operating conditions, the thermal resistance is increased by adopting the connection method of

using heat insulating cushion blocks and thermal insulating bolts to connect the H-beam to the module walls. Besides these measures, the temperature requirements of the return module in an operating orbit can be ensured with the temperature adjustment system on the ground, relying on the thermal inertia of the return module, and monitoring the orbital insertion temperature.

(B) Equipment compartment

Since the compartment walls are a thin-walled metal canopy structure and there is no fairing outside the compartment, according to thermal computations, in order to isolate and reduce effect imposed by gas dynamic heating of the ascending gas current on the temperature at the metal canopy structure of the sealed compartment, and on the instruments inside the compartment, a certain thickness of heat insulating coating layer is applied in advance, thus increasing the heat resistance between the compartment and the outside environment. The design of the thermal control coating layer outside the heat insulating coating layer is the same as that of the return module. From the results of the coating layer optimized design, the coating layer composite is adopted. At the operating state of the maximum sunlight factor, 4/20-ths of the compartment conic surface is in direct sunlight; this surface portion is coated with a material that has a relatively lower ratio of absorption to radiation (α_s/ε_H=0.35). Other surfaces are coated with material with a relatively higher ratio of absorption to radiation (α_s/ε_H=0.71) in order to control temperature level of the entire compartment, and to reduce the range of temperature fluctuations within the compartment under the operating conditions of high and low temperatures. To adjust the thermal resistance on space environment exerted by different locations inside the compartment, different thickness (10 to 30mm) of expanded plastics is cemented on part of the surface of the interior walls of the compartment, then a layer of dual surface coating aluminum thin film is cemented over all the expanded plastic interior

surface, and on the interior wall surfaces that have no expanded plastic covering. When the scheme of thermal design is decided on, consideration is given to the situation that the sealed compartment in orbit is in the state of gas-filled pressure maintenance, since the thermal insulating property of the expanded plastic corresponds to that of the multi-layer thermal insulating material, but the density of the plastic is much smaller than that of the multi-layer thermal insulating material, therefore expanded plastic replaces the conventional multi-layer thermal insulating material in all locations requiring adoption of the thermal insulating mode inside the sealed compartment. After this measure is adopted, thermal control quality is reduced; material costs are decreased; and the installation technique is simplified. On the upper and lower sealed surface outside the sealed compartment, the multi-layer thermal insulating material is wrapped in order to isolate or reduce the effect on the sealed-compartment temperature imposed by the outside environment. For instruments with little or no heat release within the compartment, thermal insulating cushion plates are used, or expanded plastics and aluminum coating thin film are applied. Alternatively, a thermal insulating layer is appropriately wrapped. Or, heat-conducting plates are laid out to transfer the heat released by instruments with high heat liberating power to instruments at lower temperature. For instruments with high power density of heating, it is required that their surface be black anode oxidized; in addition, heat-conducting silicon grease is applied to the installation surface. With these treatments, the temperature of instruments at different locations in the compartment is controlled.

(C) Instruments and equipment

For instruments and equipment (within the equipment compartment) requiring special thermal control, appropriate measures should be taken to satisfy their temperature requirements.

(1) Heat design of major payload: Steady control temperatures are required for key components of the major payload. Therefore, in addition to ensuring isothermal control accuracy, heat leaks should be reduced as much as possible in order to lower the power consumption in thermal control.

To reduce heat leaks, the heat-conducting area between component and frame should be reduced. Between metal contact surfaces, 1 to 5mm of reinforced plastic cushion plates are inserted for heat insulation. Around the outside of the heat-trapping cover, multi-layer thermal insulating material is wrapped (among other measures) so that heat is retained. To equalize the temperature of a component, radiative heat transfer should be intensified. It is required that black anode oxidation should be applied to metal surfaces within a component. Active thermal control measures for the payload include temperature control heating plates, as well as heat-sensitive electrical resistance and control wiring.

(2) Heat design for batteries: the main power supply in a satellite is represented by the chemical batteries, whose properties are as follows. There are considerable differences in dimensions and qualities for batteries, and their heat capacities also differ. Also differing are heat power, installation locations and conditions of environmental temperature. Hence, heat design should be separately conducted by blocks of batteries.

To acquire data of heat liberating power at various stages of the batteries, the amounts of heat releases are measured during the several battery operating situations. These measurements are used as the basis of heat design.

Based on the precisely known amounts of heat released by a battery, the heat equilibrium equation is used to derive different passive thermal control measures to the operating temperatures of various batteries to accommodate the operating situations of high and low temperatures in a satellite. These passive heat control measures include the following: cementing

expanded plastic and dual surface thin aluminum film on battery surfaces, and installing reinforced plastic thermal insulating cushion blocks on surfaces. For batteries with lower mean heat liberating power that operate at lower environmental temperatures, appropriate heating plates are placed inside the battery according to thermal computations based on passive heat control. After the satellite is inserted into orbit, electric heating is switched on to meet its temperature requirements.

(3) Thermal design of infrared horizontal transit instrument: the instrument is installed at the outside rear of the satellite, directly exposed to the space environment. The instrument receives solar radiation, earth reflection and earth's radiative heat flow; heat transfer exists between the instrument and satellite as radiation and conduction. There is little heat liberating power inside the instrument.

Based on the results of thermal control, thermal design of the infrared horizontal transit instrument is the mainly temperature-preserving thermal insulating design, therefore multi-layer thermal insulating material is wrapped outside the instrument, and appropriate thermal control coating layer is coated on top of the wrapping. Besides, heating plates are installed within the infrared horizontal transit instrument for electric heating in orbit in order to satisfy temperature requirements of the instrument.

(4) Thermal design of gate of sealed compartment: refer to Fig. 2; the gate extends 92^0 (in two quadrants) along the circumferential direction of the conical surfaces of the compartment. Under operating conditions with a sunlight factor ($\tau_s/\tau_0=0.75$), one side of the gate is always in sunlight at higher temperatures. The other side of the gate is always in shadow; the earth's albedo and infrared radiation received by that side are also weak, so the temperature on the gate is lower. Thus, major temperature deformations of the gate may occur in the circumferential direction of the conic surface, thus failing to seal the gate. According to the results of the thermal analysis,

two-slot aluminum heating tubes are installed on the upper and lower door frame of the gate along the conical circumferential direction to equalize the temperatures at the door frame of the gate, thus satisfying the temperature requirements along the gate circumference.

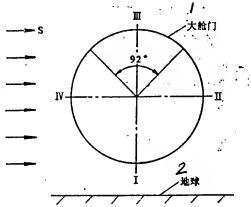

Fig. 2. Position of of sealed-compartment gate relative to sun and earth
Key: 1. Gate; 2. Earth.

(5) Temperature adjustment system on ground: for temperature control of the satellite while in the erected position just prior to launch, and to control the initial-stage temperature of satellite at orbital insertion, a ground temperature adjustment system is designed. The coolant gas line, heating plates and temperature sensors of the ground temperature adjustment system are placed in the return module and the sealed compartment.

III. Application of Thermal Inertia Method in Thermal Design

A returnable satellite has the following features: large mass, short operating time in orbit, no fairing, and low power in the return module, among others. This kind of returnable satellite is most adaptable to use of the thermal inertia method.

In thermal design, the thermal inertia method involves the satellite heat capacity. When the conditions of environmental heat change, there is a lag in temperature variations in the satellite so that the satellite-borne instruments and equipment can still maintain within the required temperature range for a certain time period. This is the thermal inertia method.

To compute the conditions of environmental heat flow, or temperature variations at satellite surfaces when its internal heat source changes, Eq. 1 is rewritten as

$$\frac{d\bar{T}}{d\tau}=(\sigma\overline{\varepsilon}\bar{T}^4-Q_{sz}-Q_i-Q_e)\frac{1}{GC_r} \qquad (2)$$

From Eq. (2), the greater the satellite heat capacity (GC_p), the smaller is the temperature variation rate ($dT/d\tau$) of satellite, and the slower is the temperature variation. Conversely, within the same time period, the temperature variation is more rapid. When considering the heat equilibrium of the isothermal nodal points on the canopy of the satellite surface, the internal power item Q_i accounts for a very small proportion of total heat flow in Eq. (2). Therefore, the item can be frequently neglected.

For the instruments within the compartment, when the internal power of the instruments, or the environment temperature change suddenly, the instrument temperature variations can be computed with the following equation.

$$Q_r+GC_r\frac{dT}{d\tau}=\frac{\Delta T}{R_i}+\frac{\Delta T}{R_f} \qquad (3)$$

In the equation,

Q_p is heat liberating power of instruments;

G is mass of instruments;

C_p is specific heat of instruments;

$dT/d\tau$ is temperature variation rate of instruments;

ΔT is temperature difference between instruments and environment;

R_i is conductive heat resistance between instruments and environment; and

R_f is radiation heat resistance between instruments and

environment.

After processing, Eq. (3) becomes

$$\frac{dT}{d\tau}=\left(\frac{\Delta T}{R_1}+\frac{\Delta T}{R_f}-Q_r\right)\frac{1}{GC_r} \tag{4}$$

From Eq. (4), the greater the heat capacity (GC_p) of the instruments, the greater is the conductive and radiation heat resistance between instruments and environment. When the internal power of instruments, or the environment temperature change suddenly, the smaller the temperature variation rate of instruments, the slower is the temperature variation of instruments. Therefore, the longer is the time to maintain a certain temperature range. Conversely, the shorter is the time period for staying within a certain temperature range.

According to the principle of thermal inertia method, and combining the unique features of the returnable satellite, thermal design is carried out in different stages of satellite operation.

(A) Applications of return module in the orbital stage

In the return module, the heat liberating power (of instruments) Q_1 is only 9W. In Eq. (1), heat transfer Q_c between the return module and equipment compartment is a negative value. According to gasdynamic heating protection, with the satellite surface coating layer under impulse, and with the thermal insulating measures possibly adopted in the compartment, computations indicate that temperature of the H-beam within the compartment is below 0^0C, unable to satisfy the lower temperature limit required by most instruments. To solve this problem, the thermal inertia method is adopted after heat analysis and computation.

The particular steps are as follows: just before launch, the temperature of the H-beam in return module is controlled by the ground temperature adjustment system so that there is greater heat quantity stored in the return module during orbital insertion. With various items (including the addition of heat

resistance in the compartment), the temperature in the compartment drops with time even though in the maximum-shadow orbit and with heat dissipating into space through the return modules surfaces, however until the final flight period of satellite, the temperature within the compartment is consistently well maintained within the required range because of the thermal inertia of the entire compartment, as shown in Fig. 3.

By using Eq. (2), we can compute the time required for the temperature of the H-beam (in the return module) or the temperature of the H-beam elsewhere to drop to different values at different satellite flight periods.

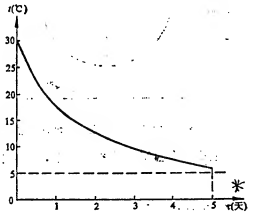

Fig. 3 Relation curve between time and temperature in return module
Key: *. Days.

(B) Applications in sealed compartment in ascent stage

Wall of sealed compartment is a thin-wall metal structure. To reduce the effect of a temperature rise on the canopy due to gasdynamic heating, a thermal insulating coating layer of a certain thickness is designed on the exterior surface of the aluminum walls of the sealed compartment. Thus, the conductive heat resistance perpendicular to the compartment surface

increases by a factor of about 130. Thus, the temperature of instruments within the compartment rises rapidly. After orbital insertion, the orbit, temperature rise lags so the temperature of instruments is up to or higher than the upper temperature limit required. As indicated from analysis and computation involving Eqs. (2) through (4), this problem can be resolved by using the thermal inertia method.

Just before launch, the ground temperature adjustment system is adopted to reduce temperature at representative points within the sealed compartment to about 5°C. In addition, this temperature level is maintained for a period of time so that the sealed compartment has a cold inertia property. During the gasdynamic temperature increase in the ascent stage, and after temperature rise lags at orbital insertion, the temperature of instruments within the compartment is still within the required range.

When a satellite is launched in summer because the environmental temperatures are relatively high, sunlight shines directly onto satellite surfaces; just before launch, the temperature within the sealed compartment is as high as 40°C. Therefore, it is especially important to apply the thermal inertia method to the sealed compartment.

If a satellite is launched in fall or winter, since the ground environmental temperature is about 5°C or below, it is not necessary to apply the thermal inertia method to the sealed compartment just before launch.

(C) Application in return module during the ground transportation stage

When a satellite is launched in summer, although the time is too short for transfer transportation stage on ground, still, the satellite transporter is in strong sunlight. In some cases, vehicle wall temperatures are as high as 70°C. Sometimes, since the instruments have been installed on board the satellite, storage or operations are required in a room temperature

environment. During ground transportation, if thermal control measures are not adopted, temperatures on these instruments and equipment may exceed the required temperature range, resulting in malfunction of these instruments. To resolve the problem of thermal control in the satellite during the ground transportation stage, the simplest, most economical, reliable and effective method is the thermal inertia method after thorough analysis.

IV. Ground Heat Tests and Flight Tests

In the satellite development stage, after thermal design was conducted upon adequate heat analysis and verifications, a series of ground tests was required, including gasdynamic heating tests of the active stage, gasdynamic impulse tests, vacuum heat equilibrium tests, and multi-flight tests, among others.

(A) Gasdynamic heating tests at active stage

The gasdynamic heating tests are tests to measure temperature increases in the canopy on the satellite surface by simulating the gasdynamic heating situation at active stage of satellite. During tests, an iodine-tungsten lamp is used to simulate gasdynamic heating thermal flow. The structure of the compartment is an 1:1 structural model. After the compartment surface is coated with the required coating layer, another black layer is sprayed and coated; expanded plastic is cemented on the interior compartment wall. During tests, variations in surface temperature are measured with an iodine-tungsten lamp to heat the sealed compartment surfaces according to a given heat-current curve.

(B) Gasdynamic impulse tests

In the gasdynamic impulse tests, an impulse is applied to the satellite model by using high-temperature gas at the flight speed of satellite in its ascent stage. Thus, the variation in the performance of thermal controlled coating layer on the satellite surface is measured.

In the tests, the two operating states of the cold blowing gas with a high pressure head, and with hot gas blowing with low pressure head, are conducted separately. As shown by the test results, the thermal controlled coating layer on the satellite surface model is perfect and sound without changes in thermal properties.

(C) Tests of vacuum heat equilibrium

In tests of vacuum heat equilibrium, the satellite is placed in the simulator in the orbital space environment (vacuum, space heat flow, and heat sink, among others) to verify whether or not the satellite thermal design of the satellite.

When deciding on a scheme for vacuum heat equilibrium of the returnable satellite, the following test methods are proposed or adopted in addition to conventional tests.

(1) Gas is admitted into the sealed compartment while in orbit. According to the results of thermal analysis, if the gas-filled state within the compartment is maintained while the vacuum heat equilibrium tests of the sealed compartment, natural convection heat transfer on ground will severely distort the test results. In the orbit, gas within the compartment is not involved in convection and heat transfer. Heat conduction of gas molecules within the compartment only occupies 4 percent of solid heat conduction and radiation heat transfer; this factor can be included in heat conduction for comprehensive consideration. Thus, it is proposed to apply tests of the vacuum state in the compartment to simulate the gas-filled state within the compartment in orbit. It is required to have adequate vacuum in the compartment during tests in order to monitor during heating tests and to ensure reality in the heating tests.

(2) In heat tests of the prototype satellite, it is required to adjust the surface coating layer of the sealed compartment in order to satisfy temperature requirements of instruments. The predetermined purpose was achieved by adopting a simulation test method without opening the vacuum chamber to change the coating

layer on the satellite surface.

(3) During the heat tests, according to the difference between the design temperature at the satellite surfaces and the measured temperature, it is proposed to computerize automatic adjustment of the infrared heating cage power to simulate outer space heat flow. By this method, the error of satellite heat equilibrium is less than 1.25 percent in an operating situation of high and low temperatures, thus ensuring accuracy of the heat tests and data reliability.

(4) During regular heat tests of the satellite, accelerated heat tests is adopted based on the results of prototype satellite heat tests.

Vacuum heat equilibrium tests of prototype satellite are conducted on the returnable satellite; this is a satellite model of 1:1 scale. Simulating instruments and electric resistances are installed in the model to simulate the heat liberating power of instruments; the infrared heating cage is used to simulate space heat flow during tests. As indicated in the test results, the thermal design can basically satisfy the required temperature range for these instruments. Based on adjusting some of the thermal control measures, regular vacuum heat equilibrium tests are conducted on the satellite. As the tests showed, the chemical batteries used in the satellite have large capacity with large amounts of liberated heat. The amount of heat liberated by the battery is measured, and thermal control measures are adjusted for some batteries. Thus, finally the thermal control technical state of satellite is determined.

V. Conclusions

(1) In the results of multi-flight operation of a returnable satellite, all temperatures of instruments in the satellite are well within the design range; in addition, the data from ground heat tests and flight tests match quite well. The repeatability of the flight data is also excellent. These facts explain that design and thermal analysis of the thermal control system are

rational; the thermal test methods and their results are effective and correct.

(2) The returnable satellite has unique features of high heat capacity, short flight time, and low heat liberating power in its return module. In the different stages of satellite operation, the thermal inertia method is an effective method of heat design. In multiple applications, good results were obtained.

(3) The coating layer design on satellite surfaces effectively controls the temperature levels in the various compartments. The thermal insulating coating-layer design on the sealed-compartment surface controls temperature rises on the compartment wall as induced by gasdynamic heating. Thus, the design indicators have been reached.

(4) A combination of passive and active thermal control techniques is adopted for major satellite major payloads. The isothermal control of temperature at key locations is reliable throughout the orbital operating period. The temperature control accuracy and power consumption are better than the design indicators.

(5) As proven in practice, special measurements and tests are conducted on the amount of heat liberated by the batteries; these results are used as the basis for thermal design of batteries. This basis is essential.

The paper was received for publication on 25 December 1989.

MAIN FACTORS AFFECTING PHOTOGRAPHIC QUALITY OF PRISM SCANNING PANORAMIC CAMERA

Yang Bingxin of Beijing Institute of Machine and Electricity

Abstract: This paper briefly presents the basic principle and characteristics of the prism scanning panoramic camera. Based on a large amount of data acquired in tests and through detailed analyses, it is concluded that the main factors affecting the photographic quality of the camera are the prism, the synchronization error between the speed of the image and that of film movement and the temperature variance. The paper also discusses how to improve the synchronization accuracy through technical approaches.

Key words: Panoramic camera, prism, resolution, synchronism, analyzing.

I. Foreword

The prism scanning type panoramic camera has unique features of large photographic area covered, compact structure, high reliability, and fast camera scanning rate, among others. This kind of camera has been extensively used in aerospace and airborne photography.

Based on development experience and experimental data with panoramic cameras, the paper presents ways of upgrading speed synchronization accuracy and photographic quality by analyzing important factors affecting speed synchronization error and

temperature variation of the prism.

II. Fundamental Principle of Prism Scanning Panoramic Camera

Fig. 1 shows the principle of the prism scanning panoramic camera.

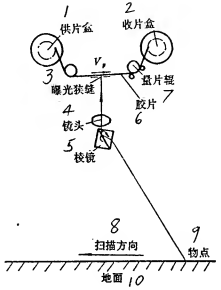

Fig. 1 Principle of prism scanning panoramic camera
Key: 1. Cassette supplying film; 2. Cassette for take-up of film; 3. Narrow slot for light exposure; 4. Lens; 5. Prism; 6. Film; 7. Roll for measuring film; 8. Scanning direction; 9. Object site; 10. Ground.

To achieve panoramic photography, two Dove prisms are placed in front of the camera lens; the rotating axis of the prism is parallel with the direction of flight. In photographing, the prism rotates and scans ground objects. From ground scenes and objects, the light passes through the prism to enter the lens. By passing through a narrow slot in front of the film, scenes and objects form an image on the moving film. For imaging clarity, the speed synchronization (equal speed and same direction) should

be maintained between the image speed generated by prism rotation, and the film travel speed. The following equations can be used to express synchronization.

$$\vec{V}_i = \vec{V}_f \tag{1}$$

$$V_i = 2\omega_p \tag{2}$$

In the equations, V_f is the film moving speed;
V_i is image speed;
f is focal length of camera; and
ω_p is scanning speed of prism while photographing.

The following unique features distinguish the prism scanning panoramic camera: synchronized motion between prism and film during photography, relatively small weight of prism, fast scanning speed, large area covered during photography, and compact structure. However, the photographic quality of this kind of panoramic camera is lower than for other kinds of panoramic cameras with the same optical parameters.

III. Factors Affecting Photographic Quality of Camera

In addition to lens and film, the major factors affecting photographic quality of prism scanning panoramic camera are the prism, the error in speed synchronization and temperature variation. There are the following secondary factors: error in film level extension, off-focusing, image shift, poor contrast with scenes and objects, control error in light exposure, and quality of photographic window, among others.

Resolution is a principal indicator in evaluating the photographic quality of a camera; the resolution is expressed with a number for convenience in comparing good results with inferior. From the standpoint of resolution, the paper quantitatively analyzes and discusses the main factors bearing on photographic quality. For example, in a certain prism scanning panoramic camera, the overall static-state photographic resolution of lens and film may reach 60 pairs of lines (high

contrast 100:1, the same in later passages) per millimeter, if the static-state photographic resolution is reduced for the camera with prism added; the resolution R_{0c} is approximately 35 pairs of lines per millimeter; the resolution R_{0a} is approximately 44 pairs of lines per millimeter along the flight direction. After the camera is switched on, owing to the influence of the synchronization error, the resolution of moving-state photography is reduced. Resolution along the scanning direction is 20 pairs of lines per millimeter in 90 percent of cases; the maximum resolution may be as high as 30 pairs of lines per millimeter, only in 50 percent of the cases. Along the flight direction, the resolution is 30 pairs of lines per millimeter at 80 percent of cases; the highest resolution is 40 pairs of lines per millimeter in 48 percent of cases. In actual operation, the photographic resolution can only reach the range between 20 and 25 pairs of lines per millimeter.

From this explanation, the lower resolution is the result of a camera employed in large prism scanning photography. These problems are discussed below.

IV. Analysis of Main Factors Affecting Resolution

For a prism scanning panoramic camera with long focal length, the prism dimensions are large with high required accuracy, difficult manufacture and assembly, as well as sensitivity to temperature. Double images will occur to place when two prisms in front of the camera lens along with reduction in light passage aperture and lowered camera resolution.

(A) Reduced light-passage aperture and lower resolution with prism added

There are unique features for double Dove prisms: if the incident light beam is circular, the exit light beam becomes two semi-circles in the reverse direction, as shown in Fig. 2. The effective aperture projected onto a circular diaphragm is reduced, thus reducing the relative aperture; this will lower

resolution to a high-grade lens (resolution approaching limit of diffraction). Visual resolution of the lens is

$$R_l = \frac{1}{1.22\lambda F} \tag{3}$$

In the equation, R_l is visual resolution of lens;

F is F number of lens; and

λ is wavelength of light.

In calculating the photographic resolution of the overall static state between lens and film we can apply an empirical formula with the addition of reciprocals.

$$\frac{1}{R_{l+f}} = \frac{1}{R_l} + \frac{1}{R_f} \tag{4}$$

In the equation,

R_{l+f} is photographic resolution of the overall static stage between lens and film; and

R_f is resolution of film.

For example, the calculated value of R_l for a lens is 175 pairs of lines per millimeter, and R_f=100 pairs of lines per millimeter. R_{l+f} is obtained in computation using Eq. (4), at 64 pairs of lines per millimeter; the actual measurement value is 60 pairs of lines per millimeter. After a prism is added, the light passage aperture is reduced by about 1/4. Therefore, the visual resolution of the camera is reduced to about 1/4; the visual resolution will be reduced from 175 to 136 pairs of lines per millimeter. According to Eq. (4), the computed photographic resolution at static-state is 57 pairs of lines per millimeter after prism is added. Owing to errors in manufacturing the prism, the resolution is lower than the calculated value.

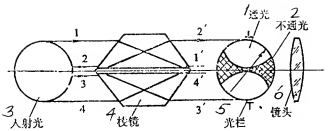

Fig. 2 Prism dividing a light beam into two semicircles
Key: 1. Light passage; 2. Opaque; 3. Incident light; 4. Prism; 5. Diaphragm; 6. Lens.

(B) Effect on resolution of prism double image

Owing to errors in prism manufacture and assembly, the incident parallel light beams become non-parallel light beams, thus forming double images on the image plane. This will lower the resolution R_{oco} in the scanning direction. The following equation can be employed to indicate the relation between the circle-of-confusion diameter and resolution:

$$R_b=\frac{2}{\Delta d}=\frac{2}{af} \tag{5}$$

In the equation, R_b is the corresponding resolution of the circle of confusion;

Δd is diameter of the circle of confusion $\Delta d=af$;

a is size of double images.

Table 1 lists values of α、Δd and R_b of a certain prism scanning camera.

Table 1 Diameter and Resolution of Circle of Confusion

α (′)	1	2	3
Δd (μm)	4.25	8.5	12.7
R_b (对线/mm)	470	235	160

Key: * - Pairs of lines.

The following equation can be used to calculate the reduction in the visual resolution of the camera due to double images:

$$\frac{1}{R_{i+b}}=\frac{1}{R_i}+\frac{1}{R_b} \qquad (6)$$

In the equation, R_{i+b} is the visual resolution of camera when double images are formed with the prism.

Owing to prism manufacture error, the actual value of R_{gc} is lower than its calculated value; generally, the actual value can reach approximately 35 pairs of lines per millimeter. Table 2 lists the calculated and the measured resolution values for various states of a certain prism scanning camera.

Table 2 Resolutions for Various States

1 分辨率 (对线/mm)	计 算 值2	实 测 值3
R_i	175	180
R_{i+b} (加棱镜相机目视分辨率) 4	76.5	77
R_{i+f}	64	60
R_{oc}	44	35～40
R_{oA}	57	44

Key: 1. Resolution (pairs of lines per millimeter); 2. Computational value; 3. Measured value; 4. Visual resolution for prism camera.

From these results of analyses and measurements, the prism reduces photographic resolution in the static state: there is a greater reduction in scanning-direction resolution (R_{0C}), approximately 40 percent, and less reduction in flight-direction resolution (R_0), approximately 1/4.

(C) Effect on resolution by error in speed synchronization

The imaging quality of the prism scanning panoramic camera

is mainly determined by synchronization accuracy between velocity of film drawing by film measuring roller, and image speed produced with prism scanning. The higher the synchronization accuracy, the higher is the dynamic resolution. Conversely, the dynamic resolution is lower. Motions of prism and film measuring roller can be mechanically driven (such as gear transmission and friction transmission). Or, electric-control circuits can execute synchronization of two velocities.

(1) Analysis on effect of resolution by error in speed synchronization

Whatever the method used in executing synchronized motion of the film-measuring roller and prism, both speeds are always changing, thus causing asynchronization of speeds. In other words, $\vec{V_i} \neq \vec{V_f}$, $V_i - V_f = \Delta V$, ΔV is called the speed difference.

Speed synchronization accuracy S_i is defined as follows: the ratio between difference (of image speed and film travel speed) and image speed (or film travel speed).

$$S_i = \frac{\Delta V}{V_i} = \frac{\Delta V}{V_f} = \frac{V_i - V_f}{V_i} \tag{7}$$

or

$$S_i = \frac{\Delta V}{V_i} = \frac{\Delta V \cdot t_{max}}{V_i \cdot t_{max}} = \frac{\Delta L'}{L} \tag{8}$$

In the equations, t_{max} is the maximum time of light exposure;
ΔL is allowable image shift generated by asynchronization; and
L is image shift.

We can see the following from Eq. (8): synchronization is determined by image shift, and the allowable image shift generated by asynchronization. Image shift is determined by image speed (or film travel speed) during photography, and by light exposure time. The allowable image shift is determined by the dynamic photographic resolution of the camera. By adopting the theory proposed by Timothy Tratt that the allowable image shift causes a reduction of 10 percent in resolution, the allowable image shift is derived by using the reciprocal square

law [1]:

$$\Delta L=\frac{1}{2R_*} \tag{9}$$

In the equation, R_0 is the static-state photographic resolution of the camera without image shift.

$$L=V_t t_{max}=2\omega_p f t_{max} \tag{10}$$

After substituting Eqs. (9) and (10) into Eq. (8), we obtain

$$S_t=\frac{\frac{1}{2R_*}}{2\omega_p f t_{max}}=\frac{1}{4R_*\omega_p f t_{max}} \tag{11}$$

As R_0=1.1R; in the equation, R is the dynamic photography resolution of the camera. Substituting into Eq. (11), we obtain

$$S_t=\frac{1}{4.4R\omega_p f t_{max}} \tag{12}$$

From the above equation, we can see that the higher the requirements on the dynamic photography resolution of a camera, the faster the prism rotation, the longer the focal length, and the longer the light-exposure time, the higher is the requirement on synchronization accuracy. Conversely, the lower is requirement on synchronization accuracy. Refer to Table 3 for the quantitative relation; resolutions are measured values.

Table 3. Light Exposure Time, Synchronization Accuracy and Resolution

t (s)	1/100	1/200	1/400	1/700
S_i	1/200	1/100	1/50	1/20
* R≥20对线/mm 所占比例	50%	60%	80%	100%

Key: * - proportion of cases when R is greater than or equal to 20 pairs of lines per millimeter.

As verified by calculations and experiments, shortening the light-exposure time can reduce the effect on resolution due to synchronization error; this is an effective approach to raise

resolution and to ensure photographic quality. Generally, the light-exposure time is shorter than 1/250 of second; usually, 1/400 of second is used.

(2) Factors affecting speed synchronization: when a gear train is used between the prism and film-measuring roller, there are following factors affecting synchronization accuracy: errors in gear manufacture and assembly, elastic deformation of shaft, and free oscillation in the gear train system, among others. This paper only qualitatively analyzes the effect on resolution imposed by gear errors.

Even though relatively precise gears are used in the gear train between prism and film, there are still very small gear errors causing speed dithering and affecting synchronization accuracy. For example, there are six levels for the gear (that engages the film to move it) accuracy. Errors in gear profile form alternately bright and dark stripes; the stripe direction is perpendicular to the film transport direction. A pair of alternately bright and dark stripes is about 5.3mm across; the frequency is about 84 hertz. Each gear generates a pair of bright-and-dark stripes. Upon scanning with a density micrometer, shape of density distribution curve is similar to that of the gear error curve.

Fig. 3 shows an amplified picture of resolution in a laboratory. There is a total of five rows of patterns. Owing to the different synchronization error at various locations, images shown in three of the rows are clearer with higher synchronization accuracy and higher resolution. Corresponding to alternately bright-and-dark stripes, the clarity of the two other rows is not as good, with low resolution and lower synchronization accuracy. Corresponding to the dark stripes, according to density difference and film contrast of the measured stripes, the maximum synchronization error can be computed.

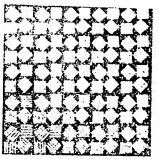

Fig. 3 Amplifying picture of resolution plate

Directly driving film-measuring roller and prism, two pairs of gears have the most effect on resolution. Accuracy should be ensured.

From this analysis, the speed synchronization accuracy of the gear train is relatively low. Even if the gear train between film-measuring roller and prism is reduced to use two pairs of fourth-level-precision gears, the dynamic resolution can only be as high as 36 pairs of lines per millimeter. [2] Hence, the gear train is not appropriate for adoption in the prism scanning panoramic camera with long focal length and high resolution. Generally, friction transmission or the electric synchronization technique is applied.

For example, the KS-120A panoramic camera adopts steel tape friction transmission (Fig. 4). In this way, the dynamic resolution is upgraded from 36 to a range between 40 to 60 pairs of lines per millimeter. The speed synchronization accuracy can be as high as 0.1 percent if precise friction transmission is employed. The dynamic resolution may be as high as 80 pairs of lines per millimeter [4] for a light-rod type panoramic camera with 610mm focal length.

For the film-measuring roller and prism, two motors are used for direct driving. By adopting the method of electric synchronization, synchronization of the two can be ensured. The precision of a steady speed between film and image can be as high as 0.25 percent. For example, electric motor driving is used in the prism of the KA-93 panoramic camera; the multi-gear train is

used for the film-measuring roller; and the mean dynamic resolution is 48 pairs of lines per millimeter (Fig. 5). After improvement, the film-measuring roller is also directly driven by an electric motor (Fig. 6). The electric synchronization technique applies to the motion between roller and prism; the mean dynamic resolution is 76 pairs of lines per millimeter (Fig. 5).

(D) Effect on resolution by temperature variation

During laboratory focus adjustment and measurement of camera, the camera temperature is approximately 20°C. The mean temperature during photography is 5°C with a difference of approximately 15°C from that during measurements and tests. The temperature variation is divided into uniform and nonuniform variations (temperature gradient). All these factors can affect camera resolution and image clarity.

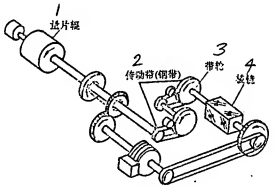

Fig. 4 Friction transmission of KS-120A camera
Key: 1. Film supply reel; 2. Transmission tape (steel tape); 3. Tape wheel; 4. Prism.

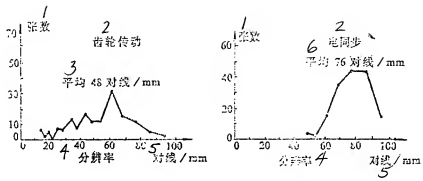

Fig. 5 Resolution curves at scanning direction
Key: 1. Number of sheets, 2. Gear transmission; 3. Average at 48 pairs of lines per millimeter; 4. Resolution; 5. Pairs of lines; 6. Average is 76 pairs of lines per millimeter.

(1) Effect on resolution by uniform temperature variation: this variation will generate stress and off-focusing on the optical parts. If the material of and the gap between lens and lens cylinder is appropriately selected, the deformation and stress of lens are very small with a 15°C temperature variation; thus, it will not affect camera resolution. The off focus quantity due to temperature can be expressed by the following equation.

$$\Delta f_T = FD(\phi_{FD} - \alpha)(T_* - T) \qquad (13)$$

In the equation, ϕ_{FD} is the coefficient of focal length at convex edge of lens;

α is thermal expansion coefficient of metal;

FD is focal length at convex edge of lens;

T_* is temperature at focus adjustment; and

T is temperature during camera operation.

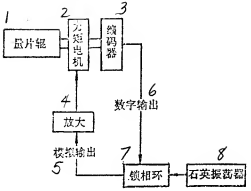

Fig. 6 Principle of improved cassette film feeding
Key: 1. Film-measuring roller; 2. Moment electric motor; 3. Coder; 4. Amplification; 5. Simulated output; 6. Digital output; 7. Phase lock ring; 8. Quartz oscillator.

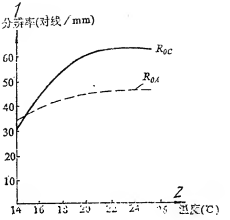

Fig. 7 Temperature affecting curve on resolution
Key: 1. Resolution (pairs of lines per millimeter); 2. Temperature.

Fig. 7 and Table 4 show the experimental results affecting resolution due to temperature variation. As indicated in experiments, the resolution is only slightly reduced when the temperature variation is 6°C; this is allowable. After the temperature is reduced to 14°C, the drop in resolution is greater, and image clarity is poorer. Among these results, the resolution R^0_A along the flight direction drops more; thus, R_{0A} and R_{0C} approach, approximately, in the range 30 to 34 pairs of lines per millimeter. By adopting the method of simulated environmental conditions for operating temperature and pressure with camera focus adjustment or by applying automatic focus adjustment, the effect on resolution can be greatly reduced due to temperature and off-focusing.

Table 4. Effect on Resolution due to Temperature Variation

2 清晰度、分辨率 (对线/mm) / T温度 (℃)	3 清晰度	R_{OA}	R_{OC}
25	4 好	63	46
19	5 较好	60	44
14	6 较差	30	34

Key: 1. Temperature; 2. Clarity, resolution (pairs of lines/mm); 3. Clarity; 4. Good; 6. Poorer.

(2) Effect on resolution due to temperature gradient: an optical system (especially the prism) is very sensitive to the temperature gradient. As discovered in experiments, camera resolution will be affected if the temperature difference at two prism terminals is greater than 2°C. Window bending and deformation will occur with off-focusing and stress if the surface temperature within camera window is between 0 and 9°C; the temperature of the exterior surface is approximately between -2 and +2°C; and the temperature difference between inner and outer surfaces is about 11°C. For thicker windows, the very small deformation can be neglected. Thermal stresses in window glass have a certain effect on resolution. As verified in experiments, it is allowable to have a temperature gradient at a window opening smaller than 5°C.

The paper was received for publication on 30 March 1990.

REFERENCES

1 Timothy Trott. The Effects of Motion on Resolution. Photogrammetric Engineering, 1960, 26 (5)
2 KA-56 Panoramic Camera Modification. AD 767908
3 Edward J Kuebert. The Fairchild KS-120A Panoramic Reconnaissance Camera System SPIE, 1974, 58: 67~75
4 Billy M Gaddy. KA-99 Panoramic Camera. SPIE, 1976, 79: 190~196

ELECTRIC POWER SYSTEM OF RETURNABLE SATELLITES

Jiang Zhujun of Beijing Institute of Spacecraft Systems Engineering

Abstract: The electric power system is one of the important subsystems of a satellite. The successful fulfillment of a space mission depends on the proper and reliable functioning of the power system.

The electric power system includes power generation, power distribution and control, and harness.

This paper first discusses the mission and characteristics of a returnable satellite, then presents a method for designing the electric power system. In particular, it describes in detail the distribution criterion, the distribution program (centralized regulation approach, decentralized regulation approach, and mixed regulation approach) and the power distributor design.

Key words: Recoverable satellite, distribution system, power divider, electric cable, electromagnetic compatibility, design.

I. Mission of Power Distribution System

The power supply and distribution system is an indispensable subsystem in various types of spacecraft. According to the work requirements of various types of instruments on spacecraft, the system provides control for power on or off. According to the work procedures of spacecraft testing, launching, operation and recovery stages, the system precisely transmits various commands

and electric signals to reliably apply electric connections to various instruments and equipment on the spacecraft. Based on the predetermined requirements, the spacecraft power supply and distribution system conducts coordination of various aspects of operations.

(A) Power supply to instruments and equipment on satellite

The main mission of power supply and distribution system is to provide power requirements at testing, launching, orbit operation and reentry of satellite.

(B) Change and control of power supply

Some parameters of power supply and electric potential available on the satellite cannot satisfy the main power supply demands of all subsystems; often, a change of power supply is required. This change of power supply can be made automatically by these subsystems, or through universal change by the power distribution system. In addition, various kinds of control on equipment on and off can be conducted by the power supply and distribution system according to satellite test and flight procedures.

(C) Channeling of commands and signals among systems

In order to coordinate all systems on a satellite to operate as per design requirements, an overall electric system is connected by the power supply and distribution system; all commands and signals are channelled and transmitted by the power system.

(D) Execute power on and off

Before its launching, a satellite is generally supplied power on the ground. During launching, power is supplied by its onboard satellite supply. There are electric-signal connections between the satellite and carrier rocket; upon entering the orbit, electric-signal separation is conducted. Signal

transmissions takes place among compartments on the satellite. At reentry, compartments should be separated. The power supply and distribution system can connect or disconnect between the satellite power supply system and the ground power supply systems, between satellite and carrier rocket, and between compartments on the satellite.

(E) Provide channel and control of ground test of entire satellite.

Among the missions of the power supply and distribution system, it provides test channels to the satellite from the ground; it conducts interswitching between ground and satellite power systems and provides power-off control during emergence.

II. Features of Power Supply and Distribution System on Returnable Satellite

A returnable satellite is different from conventional satellites in the following features.

(A) Flight time is relatively short, and power consumption is less. The orbital flight duration of returnable satellites ranges generally from several days to several months. The power supply is between hundreds and thousands of watts.

(B) There is much separation among compartments. After a returnable satellite completes an orbital mission, generally only portions of compartments of the satellite are recovered. The returned compartment is separated from the other compartments. Therefore the satellite power supply system should ensure electric connection of all compartments during satellite flight and also ensure reliable electric separation between compartments during reentry.

(C) There are many sets of firing apparatus; the ratio between the pulsed power consumption and constant loading is

high. The number of firing apparatus sets used by the recovery system and compartment separation for the returnable satellite is relatively high. The power supply system not only should provide pulsed power during operation of firing apparatus sets, but also pay attention to the safety of the firing apparatus sets and electromagnetic compatibility.

(D) Regarding the effect on the power supply and distribution system in a returnable satellite as influenced by aerodynamic heat during reentry, consideration should be given to the effect of the satellite on heat current during satellite liftoff, as well as to the high temperatures generated during atmosphere reentry of the returnable module. Necessary protection should be provided to externally exposed electric devices, plugs and cables.

III. Composition of Power Supply and Distribution System

The power and supply system of a returnable satellite includes three portions: power generation subsystem, power distribution subsystem and power supply management subsystem.

(A) Power generation subsystem

The power generation subsystem includes energy conversion, energy storage and controller. The main mission of the subsystem is generation of power, satisfying the power supply requirements by loads in the satellite. At present, the power supply used in a returnable satellite primarily includes storage battery sets, fuel cells and solar cells. What kind of power supply is to be adopted should be based on satellite service life, and load magnitudes of the payload. The simplest power generation subsystem is to employ chemical storage battery sets as power supply in the satellite.

(B) Power distribution subsystem

The power generation subsystem is the bridge between the

power supply and distribution system in the satellite and users. The subsystem is composed of three portions: power supply converters, onboard satellite distributor and onboard satellite cable network.

The power supply supplied by the onboard satellite power generation system often cannot satisfy user demands for kinds of voltage, precision and waveform factor (among other demands) for power supply. Some users require alternating current power at particular frequencies. This requires that the power distribution system supplies the corresponding power supply converters, which can be installed by users.

The onboard satellite distributor not only should accomplish conversion between ground power supply and onboard satellite power supply during ground testing of the satellite, but, in addition, the distributor should apply switch control to onboard satellite instruments, as well as power supply control on firing apparatus required by the satellite during reentry. For a rational layout of cable network in the satellite, sometimes signal- and command-switching are required through the distributor.

The onboard satellite cable network represents the "blood vessels" and links of the returnable satellite. Through the cable network, the power supply feeds every instrument in various satellite systems and organically connects signals and commands among various systems so that the systems in the satellite can be connected into an overall connected electric entity.

(C) Power supply management subsystem

The power supply subsystem is designed to apply automatic management on operation of the power and distribution system, as well as inspection of malfunctions. The subsystem is composed of parameter inspection equipment, microcomputer and software. For satellites with a simpler power supply and distribution system without a computer, this kind of work can be done by the onboard satellite electric distributor and power-generation controllers.

IV. Design of Power Supply and Distribution System

Before design and during design, there should be coordination between the overall system and subsystems for the power supply and distribution in the returnable satellite as related to all satellite subsystem components.

(A) Selection of power supply

The returnable satellite spends a relatively short period of time in orbital flight; its power is also low: little more than 100 watts for an ordinarily constant load, and 400 to 500 watts for the peak load. A chemical power supply is usually adopted.

The following chemical power supplies are employed on a spacecraft: zinc-silver storage batteries, hydrogen-nickel storage batteries, lithium cells and fuel cells, among others. Zinc-silver storage batteries are usually adopted owing to their high specific energy, reliable operation and mature production technique. Since cadmium-nickel storage batteries and hydrogen-nickel storage batteries have longer service lives of power charge and discharge than the zinc-silver storage batteries, both former batteries are used as the energy-storage power supply of solar cells. Generally lithium cells are not adopted because of their lower safety during high-power discharge although their specific energy ratio is higher than that of zinc-silver batteries. The specific energy of fuel cells is several times greater than zinc-silver batteries, therefore fuel cells are adaptable to returnable satellites and manned spacecraft with power between hundreds to thousands of watts, and operations lasting between half a month to one month. Most solar cells are used in long-service-life satellites.

(B) Power distribution criterion

The power distribution scheme of power and distribution system in a returnable satellite should meet the criteria of rationality, reliability and electromagnetic compatibility.

(1) Rationality: The technical quality of power supply and distribution should meet overall requirements; the selected voltage types of power supply and its converters should not be too many. Since low power is required by a returnable satellite, frequently a low-voltage power-supply regime is adopted. The capacity of the power supply should satisfy the power consumption requirements of various systems with a necessary surplus (generally at 10 percent) as reserve. The distances between power supply and distributor on the one hand, and the loads on the other, should be as short as possible in order to reduce power loss in transmission wires. As to the selection of power distribution devices and lead-wire specifications (and use of shields), these should be appropriate so that the power drop of wiring is controlled within an allowable range, and the weight of the distributor and cable network is not too excessive, in addition to meeting the electromagnetic compatibility requirements of the satellite.

(2) Reliability: Power distribution reliability is the prerequisite of reliability in satellite operation. In addition to reserve sufficient surplus as well as reliable power supply and its converters, it is required that reliable operation should be ensured for all components of the satellite under various environmental conditions. In distributors, all control relays should apply various controls on requirements. In cables, various connectors should ensure reliable connection to correctly transmit electric signals so that reliable separation can be ensured during separation of compartments. In addition, no obvious interference is generated to satellite attitude.

(3) Electromagnetic compatibility: For coordination on the predetermined procedures throughout the satellite without interference, the power supply requirements and load features in the various systems should be classified; systems or components with an interference source should be separated from other

systems and components. Or, individual power supplies and power-source converters should be provided to eliminate or reduce electromagnetic interference among loads. Or, the following arrangements are made: individual power supply channels, necessary shields provided, grounding or separation from the power supply.

(C) Power-distribution scheme

There are three power distribution types in a spacecraft: concentrated type, dispersed type, and mixed type. Power required by several systems are provided by a single power supply and its converters. A single main distributor is used to control power on-or-off and to connect commands; this is called concentrated power distribution as shown in Fig. 1. This power distribution scheme is very simple, only adaptable to such spacecraft with fewer systems and simple operation.

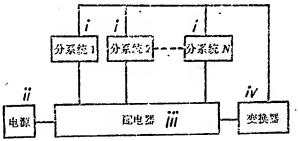

Fig. 1. Concentrated Power Distribution
Key: i. Subsystem; ii. Power source; iii. Distributor; iv. Converter.

Each system has its independent power supply, its converters and its distributors; this power distribution type is called the dispersed power distribution (as shown in Fig. 2).

In dispersed power distribution, interference among systems is low, and its electromagnetic compatibility is better than the concentrated power distribution. This scattered power distribution type has shortcomings of many power-supply sets, low efficiency in power-source converters, and large weight for the system.

With the same load features and freedom from major interference, those systems are grouped together; the power supply is provided by the same set of power supply and converters. Systems with greater interference source are provided power individually. This is called the mixed-type power distribution. Besides responsible for inter-switching between ground power supply and spacecraft power supply, the main distributor is also responsible for on-or-off control of power supply, and on-or-off control of commands in the spacecraft.

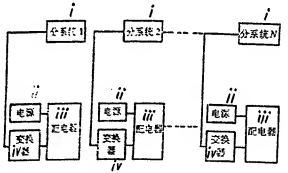

Fig. 2. Dispersed Power Supply
Key: i. Subsystem; ii. Power source; iii. Distributor; iv. converter.

In the mixed-type power distribution, the number of power-source sets can be reduced, thus beneficially raising the utilization efficiency of power-source converters. By using a large-capacity chemical power supply, the specific energy of the power supply can be increased. By sharing a set of power supplies for several systems, the power surplus can be shared

among all, thus reducing the power-supply weight of the spacecraft. A main distributor can provide on-or-off control on multiple subsystems; thus, the main distributor becomes the knob for command control in the spacecraft, thereby standardizing interface among systems so that malfunctions discovered in ground tests can be easily located and eliminated. However, for power supply to multiple systems by the same set of power supplies or by the same set of power-supply converter, power supply malfunctions can easily occur. In addition, once a malfunction occurs in a shared power supply or power-supply converter, other related systems may also have the same malfunction. Therefore, in the mixed-type power distribution, there should be high requirements on reliability of power supply, power-supply converter and subsystems. Most returnable satellites adopt the mixed-type power-distribution scheme. As proved in practice, with attention paid to reliability and electromagnetic compatibility, shortcomings of this power distribution type can be avoided.

(D) Design of distributors

(1) Layout of bus: after ground tests of the entire satellite, its launch can be allowed to proceed. A returnable satellite should pass through the following processes: launch, orbital operation and return. To have normal satellite operation with higher reliability, different buses should be laid out in the design of distributor; this is an effective and normal method.

(a) Bus testing in power supply: the power-supply buses should be routed so as to reduce interference among systems, and to be able to switch off programmed control or remote-control command when in ground testing of the satellite on a single system or on multiple systems during joint testing. This type of bus can be switched on or off by the ground test station based on test requirements. Before launch of a satellite, the power-supply buses must be connected as shown in Fig. 3.

During test procedures, K is switched off; subsystems 1 through N will not operate even with the wrong command by programmed control or remote control.

(b) Power-supply buses during operation stage: some instruments in a returnable satellite operate only after the satellite enters its orbit. To avoid wrong action by these instruments during launch, the power-supply buses during operation stage are routed. This type of power supply bus is switched off during satellite takeoff and its ascent stage. After the satellite enters orbit, the bus is connected with multiple commands (such as programmed control and remote control) as shown in Fig. 4.

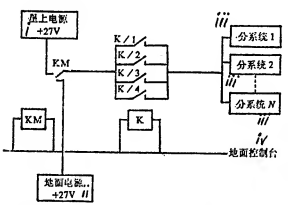

Fig. 3 Power supply test bus

Key: i. Satellite power supply; ii. Ground power supply; iii. Subsystem; iv. Ground control station.

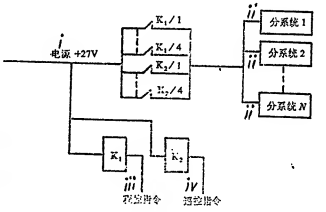

Fig. 4. Power-supply bus at operation stage (or return stage)
Key: i. Power supply; 2. Subsystem; iii. Programmed-control command; iv. Remote-control command.

(c) Power-supply bus during return stage: during launch and orbital operation, both the recovery system and the related firing apparatus in a returnable satellite do not operate. In this type of system and equipment, the power-supply bus during

the return stage is routed. This type of power-supply bus is connected only when operation is required on recovery system and firing equipment before satellite reentry. The control method is the same as shown in Fig. 4.

(2) Design of control wiring: there are the following primary control functions for the distributor in a returnable satellite.

(a) Interswitching between ground- and satellite-power supply;

(b) Power distribution and supply control by the power supply;

(c) Triggering control of firing apparatus in the satellite;

(d) Electricity separation control of separation connectors among various modules of the satellite (and between the satellite and its carrier rocket); and

(e) Command control (and other activities) during ground testing of the satellite.

While designing distributor wiring, we should base our work on the requirements for power supply voltage and power consumption (as well as characteristics of load, system operation procedures, and different control requirements) of power supply objects to select circuitry and components. If the wiring is used to control the switching and control of the power-supply bus, generally magnetic self-locking relays are adopted. In the power-supply control circuits that are frequently switched on and off, electromagnetic relays of different power ratings can be adopted.

The loading capacity at contact points in the relay should be larger than the actual loading. Owing to asynchronization in the operation of different contact points in the same relay, we cannot apply contact-point parallel connection to increase electric current because this may damage the relay contact points.

In the case of important control commands, the contact-point

parallel control mode with dual-point dual-line and multi-command multi-relay should be adopted in order to enhance reliability.

(3) Protection of interface circuit: the main control component in a distributor is the relay. When the power is off in relay circuitry, a higher counter-electromotive force will occur. Therefore, a protective circuit should be added to both terminals of relay circuitry. In addition, the value of the resistance in relay circuitry should adapt to its loading capability in order to avoid damage to the interface circuit.

(4) Protection of power supply, and design of electromagnetic compatibility: in a returnable satellite, the distributor should exercise power-supply control on multiple systems; a power supply set often supplies power to multiple systems. Therefore we should pay attention to the protection of power supply, and to design of electromagnetic compatibility. Protection can be realized by connecting in series the current surge protective components (or circuits) in the power-supply circuits of various subsystems. Necessary measures should also be adopted on the sections easily subject to current surges in distributor design.

To enhance electromagnetic compatibility of control circuits, there should be isolation between the power-supply control of loads in different magnitudes; different relays should be used for control. When a single power supply is shared by several systems, it is best to isolate the control relays (even the power supply of these systems can be simultaneously switched on or off) to reduce inter-system coupling. Moreover, common terminals should be connected to the power supply terminals as shown in Fig. 5.

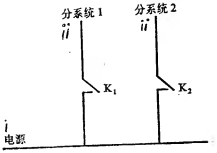

Fig. 5. Rational control mode
Key: i. Power supply; ii. Subsystem.

(E) Cable network

Design on cable network in a returnable satellite should be conducted on the following requirements.

-- Requirements on cable network by the overall layout, structure installation and module separation in a satellite;

-- Electric connection wiring diagram, contact-points distribution table, and requirements on power supply and transmission wire for equipment in various subsystems;

-- Requirements on power supply and distribution as well as on grounding wires in a satellite;

-- Requirements on cable network in terms of satellite reliability and electromagnetic compatibility; and

-- Requirements on performance and indicators of cable network for the satellite, from an overall point of view.

The following problems should be taken note of cable network design.

(a) Treatment of grounding wires: in a returnable satellite, the power supply circuit is of two-wire system type; the satellite shell is not used as power-supply ground or signal ground. The datum ground of the satellite can be considered at

the negative pole of the power supply, or the common ground near the negative pole of the power supply. Systems with high interference should be placed independent, if possible. Grounding of the shielding layer of cables and installation wires should be placed on grounding points according to requirements.

(b) Design of branches of cable network: the cable network is composed of n cables; each cable can have multiple branches. For convenience in installation, the exterior connections of a single electric connector should not be too numerous. Or, if necessary, electric adapter connectors are installed for isolation.

(c) Selection of electric conductors and lead wires: as adopted in a cable network, electric connectors should be as few in number as possible with limited model numbers and specifications. Among modules, electric isolators and connectors are key components affecting the success or failure of satellite reentry; they should be very reliable. These separators should enable separation (both electric and mechanical separation) in high vacuum and before satellite reentry. While still in the recovery module after separation, electric sockets should have flame-protective shields; ablation protective measures should be carried out externally to the sockets. Humidity-proof properties of lead wires in the cable network should satisfy the environmental conditions of cable operation. With respect to lead wire size, consideration should be first given to the current capacity of each lead wire in a cable bundle, and also to satisfying the potential drop requirement of various systems. For cable bundles with high current or pulsed power supply, double twisted wires or double twisted shielded wires should be used. During cable installation, isolation from other cable bundles should be ensured; in addition, connection with various types of grounding wires should be satisfactory.

The paper was received for publication on 13 August 1990.

1579

REFERENCES

1 Chetty P R K. Satellite Technology and Its Applications. TAB Books Inc., 1988.
2 Ivan Bekey and Daniel Herman. Space Stations and Space Platforms-Concepts, Design, Infrastructure, and Uses. Progress in Astronautics and Aeronautics, 1985, 99
3 Koelle H H. Handbook of Astronautical Engineering. McGraw-Hill Company, Inc., 1961.

DEVELOPMENT OF RETURN TECHNOLOGY AND RETURNABLE SPACECRAFT

Wang Xiji of Chinese Academy of Space Technology

Abstract: According to the statistics of launched spacecraft, the number of returnable spacecraft. Returnable spacecraft play a pioneering role and make a great contribution to manned spaceflight and human progress. The paper analyzes in detail three phases of the development of return technology and returnable spacecraft, namely: the preliminary development phase, the application phase and the nondamaged fixed-point return phase, and points out that it is the nondamaged fixed-point landing return that will become the main development approach for quite a long period in the future.

Key words: Recoverable satellite, return technology, development.

I. Return Technology and Important Status of Returnable Spacecraft

Generally speaking, mankind's aerospace activities can be divided into two major categories: the first category covers activities of exploring and understanding outer space; the other category covers activities of exploiting and utilizing resources in space. Among the activities of exploring and understanding the space, in many cases the activities should enable specimens to be returned from space, as well as test specimens and objects to be sent into space and brought back, in addition to acquired

information to be returned for processing, analysis and research. Among the activities of exploiting and utilizing resources from outer space, objects for space experiments, preparation and production should be returned to ground for their own actual value besides information acquisition, transmission and relay. Among the two above-mentioned categories of aerospace activities, when the amount of the acquired information is huge, or when it is not feasible to send or receive this information, it can be stored on a medium (film, magnetic tape, optical disk, etc.) and the medium returned to the ground in order for retrieval information. Whether it is specimens, test samples or objects recovered from space for ground experiments, preparation or production, or a medium with information stored for retrieval, we should rely on return technology and utilize returnable spacecraft.

In the two categories of aerospace activities, manned aerospace activities are quite significant. As the center of manned aerospace activities, this includes man's entry into outer space, exploitation of man's mobility and initiative to promote advances in aerospace achievements and to contribute to progress for society and better living standards. When humans are in outer space, they should return to ground once the mission is accomplished or an emergency occurs. Therefore, return technology and emergency rescue techniques (as an obligatory element in return technology) are key factors that should be mastered in fostering manned aerospace accomplishments. Almost all types of manned spacecraft are returnable spacecraft. In some special manned spacecraft, a manned space station and a deep-space base are not returnable spacecraft; however, some returnable spacecraft should be available for service to the station or base.

Based on statistics, about one-third are returnable spacecraft, of all spacecraft previously launched in the world. Up to the early 1990s, there have been 11 returnable satellites out of the 26 successfully launched by China; this is 42 percent

of all launches. Thus it can be evidently seen that return technology and returnable satellites are prominent in overall aerospace advances. Up to the present time, only three countries (Soviet Union, United States and China) have mastered return technology and have capabilities of launching returnable spacecraft. Of more than 1000 returnable spacecraft previously launched, all were launched by the three above-mentioned countries. Thus, these three countries have a unique status in world aerospace activities.

From the standpoint of exploiting and utilizing space resources, returnable spacecraft serve as pioneers and leaders. The world's first satellite application system (the Explorer satellite reconnaissance system launched by the United States) is an application system of a returnable satellite. In addition to the United States, the first satellite application systems of Soviet Union and China were also returnable satellite systems. All future exploitation and use of microgravity resources and space energy sources rely on return technology and returnahle spacecraft. If a country does not develop and master return technology, it will be restricted and hindered in many aspects of aerospace activities. In other words, that country will find it difficult to establish and develop its independent aerospace capability. Up to the late eighties, therefore, almost all major aerospace countries regarded return technology as the key to further gains in aerospace; the technology is included among the major aspects of aerospace for development. In this respect, China was fortunate enough to foresee this trend two decades earlier than West European countries and Japan. Of course, we should make good use of this acquired technology, capability and initiative status to make progress in aerospace.

II. Development of Return Technology and Returnable Spacecraft

Return technology and returnable spacecraft are developed in response to the demands of aerospace activity. The development procedure can be generally divided into three stages.

(1) Breaking the bottleneck of return technology for the safe return of the return module (the general term for all that is returned in a returnable spacecraft) with its payload. This stage can also be called the initial stage.

(2) This is the stage of extensive application and development of the single-use return module in aerospace activity; this stage can also be called the application and development stage.

(3) This is the stage of developing nondamaged or fixed-point landing return technology and the return module.

The second and third stages are a continuation of the first stage. Subsequently, both later stages continue sustaining the trend of parallel development. Below is an explanation of these three development stages.

(1) Initial stage of development

After the successful launch of the first artificial satellite on 4 October 1957, the value of outer space was sharply upgraded. To obtain benefits from aerospace activities as fast as possible, for example the acquisition of intelligence with excellent conditions of satellites in outer space orbit not restricted by national boundaries, both the United States and the Soviet Union placed the breakthrough of return technology and development of returnable spacecraft as major points of development.

This breakthrough of return technology was achieved by both the United States and Soviet Union at about the same time of August 1960. In this period, the United States successfully returned and recovered the return module (carrying live specimens) of the Explorer Satellite from near-earth orbit; the Soviet Union also successfully returned and recovered the return module (carrying live specimens) of Sputnik 5 [1]. In August 1960 (only about eight years after the launch of the first satellite), both the United States and Soviet Union achieved this breakthrough progress within this short period of time. In

addition to their vast investment and huge efforts, there are two important factors.

(a) Both the United States and Soviet Union achieved at that time certain level of two technical aspects (atmospheric reentry of guided missile warheads, and recovery technique with parachute recovery of rocket nose-cones. Beginning in the forties, both countries began to develop guided missiles and sounding rockets. In the fifties, both countries were able to recover rocket nose-cones descending from a trajectory with peak elevation between 200 and 300km in altitude.

(b) Both the United States and Soviet Union pursued the route of breakthrough and mastery of return technology in developing the ballistic type reentry return module with simple aerodynamic exterior, more convenient solution to the thermal insulation problem, and lack of control after leaving the operating orbit.

By summarizing both these points, this represents adequate use of the available technical foundation and selection of a correct technical route. This is possibly why countries achieved successful efforts within a short period of time.

Although the United States and Soviet Union are in the early period of developing aerospace technology, and in mastering the ballistic type return technology within a short period of time, yet it should not be considered that mastery of this technology is relatively easy. Comparing with nonreturnable type spacecraft, returnable spacecraft have an added return procedure in their missions. Quite a few special systems and some equipment sets are required in order to accomplish the return procedure. To an spacecraft, the environmental conditions confronted during the return procedure are more complex and undesirable than those during the launch process and operation process. Hence, mastering return technology and development of the returnable spacecraft are, relatively speaking, a much more difficult topic than the development of nonreturnable spacecraft.

(2) Stage of extensive application and development

After successful development of ballistic type returnahle spacecraft, these spacecraft have been extensively applied. The reason is not only that this type of spacecraft is the first type of returnable spacecraft; more important is its simple structure, high reliability and good economic features, besides its adaptation of multiple requirements. Therefore, launch and application of some ballistic-type returnable satellites have been continuous from the sixties to the present. In the early sixties, manned spacecraft also adopted the ballistic-type return module. The ballistic-type return module also has some major shortcomings as follows: excessive overloading due to fast aerodynamic speed reduction during reentry, too narrow a reentry corridor, overly great overloading due to increasing reentry speed during reentry by applying parabola orbital speed, and an overly broad distribution area for landing points. These shortcomings cannot satisfy the technical requirements of manned spacecraft and such spacecraft returned from the moon. This situation promotes the development of trajectory-lift force type spacecraft as an improved version of ballistic-type reentry. In March 1965, the United States launched and successfully recover the Gemini 3 manned spacecraft; this is the world's first ballistic-lift force reentry spacecraft. The Gemini uses a moderate lift force generated by flat angles of attack, thus considerably improving the return performance of the spacecraft. Compared with the ballistic-type reentry Mercury manned spacecraft of the United States, the reentry angle is increased from 3^0 to 7^0; the maximum overloading is reduced from 10g to less than 5g; and the distribution of possible landing points is reduced from 100-km magnitude to 10-km magnitude. After the Gemini manned spacecraft, the Apollo spacecraft of the United States, the Soyuz, Soyuz-T and Soyuz-TM spacecraft of the Soviet Union are all ballistic-lift force type manned returnable spacecraft.

The Soyuz-TM of the Soviet Union was launched in 1986 as the

most recent generation of manned spacecraft. The year 1986 is 21 years after the launch of the first Gemini; however, both spacecraft adopt the same kind of ballistic-lift force reentry return module. Thus, a conclusion can be drawn: the ballistic-lift force type return module can satisfy the fundamental requirements of manned spacecraft. It is visualized that ballistic-lift force type will be applied in the future manned spacecraft or similar spacecraft, such as orbital life craft.

With an atmosphere reentry speed approaching or greater than the parabolic orbital speed, the reentry module has been developed on the basis of the projectile-lift-force reentry technique. The first such spacecraft was Sounder 6, launched by the Soviet Union in November 1968. After escaping from moon orbit, the Soviet spacecraft directly entered the earth atmosphere approaching the second cosmic speed. The reentry module of this craft is a projectile-lift-force reentry module with a skipping reentry pattern in atmospheric reentry. The Apollo manned spacecraft and the Soviet Lunakhod are reentry type spacecraft directly entering the earth atmosphere after escaping lunar gravity; both craft are projectile-lift-force spacecraft. In addition, all spacecraft launched by the United States and the Soviet Union in directly entering the gravity of Venus and Mars are projectile-lift-force spacecraft. With increasing human interest in other planets besides the moon and earth, there are good development prospects for this type of spacecraft.

III. Development Stage of Nondamaged Fixed-point Landing Reentry Technique and Reentry Module

After completing its orbital mission, the returnable spacecraft or its module, the reentry module, can return to earth. This phenomenon naturally induces a problem (by researchers) of whether the returned reentry module can be launched again. As to the one-time use aspect of spacecraft, this problem is the repeated-use problem of a spacecraft or its reentry module. Obviously, such a spacecraft can be again

launched for an orbital mission after reentry and it must be a spacecraft that is free of any damage during orbital operation, reentry and landing; only such a spacecraft can accomplish repeated and multiple uses. Such repeated use renders great economic benefits to aerospace ventures; this is one of the long-term targets pursued by aerospace designers. For repeated use of spacecraft, numerous technical problems should be solved; however, the key problem is the nondamaged and fixed-point landing reentry technique.

There are two, different routes for the development of nondamaged and fixed-point landing reentry technique. One is the development of winged lift-force type reentry module; the other is the development of a deployable aerodynamic-wing reentry projectile-lift-force type reentry module. For development along the first route, there are the space shuttle of the space transportation system in the United States, Soviet's Buran, and Hermes of West Europe, among others. For development along the latter route, there are the Gemini spacecraft of the United States, Cheops reentry type satellite system [2] of the General Electric Corporation in the United States, and Service reentry type satellite system [3] of the North Industrial System Corporation of the United Kingdom, among others.

There are already two types of winged lift-force reentry module: the Space Shuttle of the United States and the Buran of the Soviet Union. In both craft, they have solved the problem of horizontal fixed-point landing technique on a runway, and the problem of basically solving the nondamaged reentry technique. However, in both craft the 100 percent nondamaged return is still beyond the expected target, which is the capability of repeated launch after inspection. For the case of the winged lift-force type reentry module, its structure is complex in shape; the reentry route is long; and the overall amount of reentry heat received is high. In order to reach the 100 percent undamaged return and fixed-point horizontal landing, complications are added to aerodynamics, structure, heat prevention, control,

guidance and return site. In the case of the U. S. Space Shuttle, although after 11 years of operation and an investment of about 20 billion American dollars with the successful development in 1981 of the Space Shuttle for routine operations, yet there are still numerous problems. In particular, the capability of nondamaged reentry technique is still beyond reach, incapable of being launched again after being inspected. Therefore, maintenance and operation expenses are very high, unable to exhibit the advantages of repeated usage. For the winged lift-force reentry module, much work remains to be done in order to demonstrate its repeated-use economy.

For the reentry projectile-lift-force return technique of the deployable aerodynamic wing, in the sixties the technique was exhibited in the development of Gemini spacecraft. Eventually the scheme was not adopted. At that time, a rigid deployable aerodynamic wing was adopted in the reentry process. In the late eighties, interest on this technique revived; China was one of those interested in expressing high interest in this technique. In China, many proposals and schemes were raised; a large number of experiments was conducted. At that time, the rigid deployable aerodynamic wing was not adopted; the ramjet type wing parachute was adopted. Up to now, however, not a single model has been developed. The cause of failure in the development may be the excessively high hope placed on the winged reentry module by the world's aerospace experts. Since the United States places its prospect on aerospace ventures almost solely on the winged repeated-usage Space Shuttle, a consensus has been created; it seems that only the winged reentry module can solve the problem of nondamaged and fixed-point landing technique, thus becoming a repeated-usage reentry type spacecraft. In this environment, the development of wing parachute recovered projectile-lift-force type reentry module was placed on a low priority with slow development. Only in the late eighties, after problems with the Space Shuttle were exposed, did the world's aerospace experts again pay attention to the available projectile-lift-force type

reentry technique.

It can be expected that within a considerable period of time in the future, parallel development will be proceed with the nondamaged fixed-point landing return technique along both routes: winged lift-force type return, and wing parachute recovered projectile-lift-force return. Two types of repeated-use recovery spacecraft will appear.

The paper was received for publication on 2 5 August 1990.

REFERENCES

1. Bureau of New Technology, Chinese Academy of Sciences, Brief Information on Artificial Satellites, Spacecraft and Cosmic Rockets Launched by the World Countries Between 1957 and 1964, Beijing, Science Publishing House, 1965.

2 Mayer P T.A Cyclically Harvested Earth/Orbit Production System,AIAA 84-1450.1984.

3 Bulloch C,Materials Processing, Back to Ballistics,Interavia, Nov.1986,1313

CHINA'S RETURNABLE SATELLITES

Min Guirong and Lin Huabao; both of Beijing Institute of Space Technology

Abstract: China's returnable satellites is a type of low orbit and three-axis stabilization with the feasibility of safe recovery of the return module. These satellites can be used as remote sensing satellites, micro-gravity experimental platforms, as well as satellites for scientific and technical experiments. The paper briefly outlines various subsystems, launching, return and major applications of these satellites. Up to 1990, China has successfully launched and recovered 12 returnable satellites with good social and economical benefits.

Key words: China, Recoverable satellite, Outline.

I. Foreword

Up to 1990, there have been 12 returnable satellites (refer to Table 1) among satellites successfully launched in China. These are a type of application satellite with the most launches and relatively high social and economical benefits. All these 12 satellites were launched by China's Changzheng No. 2 C carrier rockets. After operating in orbit for 3 to 8days, they were recovered in inland China.

China's returnable satellites are a type of low orbit and three-axis stabilization satellite with the feasibility of safely recovering the return module. The total weight of a satellite is

1800 to 2100kg, composed of more than 10 subsystems. This type of returnable satellite can be used for remote sensing satellites, micro-gravity experimental platform, and satellite for scientific and technical experimentation.

In November 1975, for the first time China successfully launched and safely recovered a returnable satellite. In seventies, a total of three satellites was successfully launched; eight satellites were launched in the eighties. This is the first year of nineties: another satellite was launched obtaining large amounts of very valuable information.

Table 1 Major Parameters of China's Returnable Satellites

卫星序号 1	发射日期 2	返回日期 3	起飞质量 (kg) 4	近地点 (km) 5	远地点 (km) 6	周 期 (min) 7	轨道倾角 (度) 8
中国4号 9	1975.11.26	11.29	1 800	181	49	91.2	63.0
中国7号 9	1976.12.7	12.10	1 800	172	492	91.2	59.5
中国8号 9	1979.01.26	01.29	1 800	169	488	91.0	57.0
中国12号 9	1982.09.09	09.14	1 800	177	407	90.2	63.0
中国13号 9	1983.08.19	08.24	1 800	175	404	90.2	63.3
中国16号 9	1984.09.12	09.17	1 800	178	415	90.3	68.0
中国17号 9	1985.10.21	10.26	1 800	175	409	90.2	63.0
中国18号 9	1986.10.06	10.11	1 800	176	402	90.2	57.0
中国20号 9	1987.08.05	08.10	1 800	172	410	90.2	63.0
中国21号 9	1987.09.09	09.17	2 100	208	323	89.7	63.0
中国23号 9	1988.08.05	08.13	2 100	208	326	89.7	62.8
中国30号 9	1990.10.05	10.13	2 100	206	308	89.6	57.1

Key: 1. Sequence number of satellite; 2. Launch date; 3. Recovery date; 4. Takeoff weight; 5. Perigee; 6. Apogee; 7. Period; 8. Dip angle (in degree) in orbit; 9. China, No.

II. General Descriptions of Various Subsystems in Satellite

In the case of the FSW-1 returnable satellite, its exterior appears as a composite of a spherical crown and a circular

platform with a 10° semi-conical angle, as shown in Fig. 1. The maximum diameter at base is 2.2m; its overall length is approximately 3.1m; and its total weight is between 1800 and 2000kg, depending on different payloads. In its powered flight stage, there is no protection of a rectifying canopy outside the satellite.

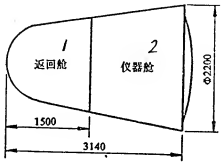

Fig. 1 Exterior of China's FSW-1 returnable satellite
Key: 1. Recovery module;
2. Instrumentation module.

Including payload, a satellite is composed of 12.subsystems: structure, heat control, compartment-pressure control, attitude control, programmed control, remote control, remote sensing, tracking sending, power supply and distribution, antenna, recovery and payload.

There are two modules in a satellite: instrumentation and recovery modules. The instrumentation module is divided into two portions: transitional and sealed compartments. All satellite-borne instrumentation and equipment are installed within the instrumentation and recovery modules. After the satellite performs a specified mission in its orbit, the recovery module is separated from instrumentation module. Acted on by the retro-rocket, the recovery module leaves its original operating orbit to enter the atmosphere and safely return to ground. However, the instrumentation module operates continuously in orbit, which will gradually decay, eventually falling into the dense

atmosphere to burn and be consumed like a meteor.

The following is installed in the recovery module: recovered portion of payload, and instruments and equipment related to satellite recovery, such as the recovery subsystem, portions of power supply and distribution, tracking orbit sensing and remote sensing subsystems, among others. The exterior layer of the recovery module is a thermal protection structure, capable of withstanding severe gas-dynamic heating during reentry in order to protect instruments and equipment within the module.

The following instruments and equipment are installed within the instrumentation module since they operate only in orbit and are not required to return to ground: all subsystems of attitude control, programmed control and module pressure control; major portions of remote sensing, tracking sensing as well as power supply and distribution subsystem, in addition to portions of payload and remote control subsystem. Among these instruments and equipment, gas bottles and lines of attitude control and compartment-pressure control are installed in the transitional stage. The execution mechanism of attitude control, as well as earth and solar sensors, are installed outside the instrumentation module base; other instruments and equipment are installed within the sealed compartment. The internal pressure of the sealed compartment is kept constant by a compartment-pressure control system.

The mission of the heat-control subsystem is to provide the thermal environment for normal operation of all instruments and equipment in the satellite through a series of heat-control measures. Based on the unique features of short service life and low orbit of a recovery satellite (combining with the actual situation of the satellite), passive-type heat control is primarily used throughout the satellite. Active heat control is supplementary to instruments and equipment with special requirements.

In the case of passive type heat control, the following modes are adopted: multi-layer wrapping of thermal-insulating

materials, thermal insulation and portions of the heating pipes. In the case of individual equipment with severe requirements of temperature environment and controllable electric heating, local active-type heat control is applied. Temperatures throughout the satellite are controlled within a range of 0^0 to 40^0C.

The mission of the attitude-control subsystem includes the following: (1) elimination of initial deviation generated during separation of the satellite from its carrier rocket; (2) during the stage of orbital operation, satisfy the requirements of attitude and the attitude angular velocity required by orientation to earth; and (3) before the satellite returns to the ground, establish the orbit separation attitude required by the retro-rocket thrust vector.

The attitude control subsystem relies on digital control with a computer, by adopting an attitude measurement system composed of a liquid floating-rate integrating gyroscope, an infrared earth sensor, and a digital type sun tracker. When determining an attitude measurement value, a Kalman filter is adopted. The onboard computer computes real-time orbital parameters and processes data. The execution mechanism adopts a cool gas reaction jetting system. The attitude control precision of pitch, as well as roll is better than 0.7^0. The control precision of deviation-flight attitude is better than 1^0.

The programmed control subsystem provides operational procedure commands to the satellite when it operates in orbit. The command is controlled by the onboard computer, which sends commands to various switching units and to operations so that the satellite can accomplish predetermined work in orbit. The programmed command controlled by the programmed control subsystem is programmed in the satellite before its launch. After the satellite enters orbit, new programs can be fed to the satellite from the ground through a remote control subsystem to revise the previously installed programs based on actual requirements.

Moreover, an onboard clock is installed in the programmed control subsystem; the clock can provide information on standard

time in the satellite.

The remote control subsystem is an active type control mode for satellite work. A ground station sends various remote control commands to the satellite for necessary control and management on satellite operation. The remote control command includes commands to switch on or off the related units in the satellite and operation command. A considerable portion of the remote-control command is the command in reserve for programmed control and the recovery time procedure mechanism. In addition, the remote control subsystem can feed new data to the onboard programmed control subsystem based on orbital parameters actually measured.

Coordinating with ground tracking stations, the tracking and orbit sensing subsystem tracks and measures the satellite orbital parameters in real time. The installation of a microwave single pulse radar responder system (including a homing signal indicator) and an ultra-shortwave velocity and distance sensing system on the satellite constitutes a tracking system mutually independent and reserved for instant use.

According to orbital parameters actually measured by the ground tracking station, the orbits predicted in the near future to the last orbit can be made in predicting the actual satellite orbits. According to the orbital parameters actually measured, the programmed control data (in the satellite) can be revised as necessary. In addition, the satellite touchdown location can be predicted.

In timely fashion, the remote metering subsystem sends to ground the actual operation parameters of various satellite subsystems; this is a digital type remote metering system. In the orbital operating stage, there are two measures: real-time remote metering and delayed remote metering. When the satellite flies beyond the ground station range, the processed data thus obtained are stored in memory as RAM. When the satellite enters the ground station range, the memory is read out at a relatively high code rate; the modulated data are then sent to the ground

station.

At the return stage, there are two measures of real-time remote metering and recovery magnetic recording. In the latter, various measured parameters of the return process are recorded in the recovery magnetic memory recorder on the satellite. The memory recorder is read out after the return module lands safely.

The power supply and distribution system provides the primary and secondary energy supplies to subsystems on the satellite. The primary energy source consists of chemical-energy batteries; the secondary energy source serves to convert the primary energy source into operating voltage as required by instruments and equipment. In addition to providing the required power supplies to the satellite instruments and equipment, the distributor relays various control commands and transmits various sensing parameters.

The return subsystem includes two portions: retro-rocket and recovery system.

The retro-rocket is a rocket engine (using solid propellant) with spherical-shaped combustion chamber. The retro-rocket provides particular velocity increments along the predetermined braking direction for the satellite return module, so that the return module can leave its operating orbit for insertion into a return orbit for entering the dense atmosphere.

The recovery system is composed of a parachute system, a firing unit, a recovery programmed control mechanism, and a locating unit. The main mission of the recovery system is to that the return module lands safely at a specified velocity. Moreover, locating information is released during the descent and after landing, so that the ground search personnel can discover as early as possible the orientation of the return module for timely organization of the recovery.

The parachute system has two portions: drogue chute and main chute. Two-stage speed reduction is carried out on the return module for ensuring safe landing. The locating unit is mainly based on radar; on the satellite there is installed a recovery

radar responder, an ultra-shortwave signal indicator, and a medium-wave signal indicator for search orientation by ground personnel.

III. Launch and Return of Satellite

Returnable satellites are launched by Changzheng No. 2C carrier rocket. The launch site is the Jiuquan Satellite Launch Center located in Northwest China.

After a satellite enters orbit, sensing control and flight management (including return control, as well as search and recovery operation in the recovery zone) are conducted by the Xi'an Satellite Control Center.

The satellite adopts a ballistic type reentry approach. In beginning the recovery, first the attitude control system on the satellite adjusts the satellite attitude as required by retro-rocket operation. Then the return module separates from the instrumentation module.

With the firing of the retro-rocket, a predetermined velocity increment is applied to the return module, which flies in a new synthesized vector to enter a transitional orbit capable of intersecting with the earth's dense atmosphere. After the return module enters the dense atmosphere, its velocity is rapidly reduced under the action of gasdynamic drag. When the descent in at an altitude of 15km, the return module velocity drops to less than the speed of sound. At this point, the recovery system begins to operate.

During the operating procedures of the recovery system, first the rear thermal protection bottom cover of the return module is ejected. Simultaneously, the ultra-shortwave and medium wave signal indicators of the recovery radar responder in the return module begin operating. Successively, the drogue chute and the main chute open up one after the other for the safe landing of the return module.

Previously installed in the recovery zone, a radar sends interrogation signals to the return module. Based on echoes of

the radar responder on the satellite, the orientation and distance of the return module can be determined. Over the recovery zone, several helicopters (equipped with ultra-shortwave directional compass) can determine the orientation of the return module while in air and upon landing. These helicopters fly in the direction indicated by the directional compass until the target is discovered. In addition, ground search personnel can determine the orientation of the touchdown point of the return module based on their portable medium-wave directional instrument.

IV. APPLICATIONS OF SATELLITE

Space remote sensing is one of the applications of China's returnable satellites. As a payload for this type of satellite, the Chinese Academy of Space Technology developed space-borne visible light cameras of different types and different purposes, such as the panoramic scanning camera, nodal-point type panoramic camera and sheet-type large picture camera for photographing ground, as well as the star camera for photographing stellar space. In flight tests, good results have been obtained.

When employing these satellites in a general survey of resources in the national territory, the features of satellite pictures thus obtained are relatively large scale, clear pictures, relatively high gray scale, wide visual field and fast speed, among others. The ground resolution considerably exceeds the scanning pictures obtained by ground satellites and meteorology satellites.

While applying this type of satellite on photographic surveying, the pictures thus obtained can be used to prepare maps, thus providing advanced techniques for China's cartography technology. After evaluation by Chinese experts, their view is that China's satellite photography surveying techniques have entered the world's advanced ranks.

The returnable satellite is also used in micro-gravity scientific research in space with good results. On the four

returnable satellites launched between 1987 and 1990 by China, 222 items of micro-gravity experiments were conducted. In addition, the following micro-gravity experimental services are provided users from France and Federated Germany: seaweed culture, protein growth and surveying of micro-gravity environment, among others.

Very satisfactory results were obtained in all these research areas. In particular, the results from experiments on forming arsenic gallium single crystals in a space materials treatment furnace, impurity-free arsenic gallium crystals, complete structure and uniform composition ratio. The results are of high scientific and economic value.

To meet requirements of ever-increasing micro-gravity research in China and abroad, the Chinese Academy of Space Technology makes available to users in China and abroad two types of micro-gravity experimental platforms (FSW-1 and FSW-2 as shown in Table 2 and Fig. 2) based on the present models of satellite.

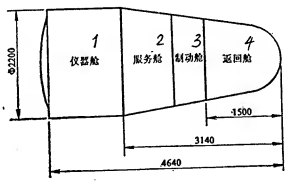

Fig. 2 Exterior of FSW-2 micro-gravity platform
Key: 1. Instrumentation module; 2. Service module; 3. Retro-model; 4. Return module.

Table 2. Two Types of Micro-gravity Platforms Commercially Available

主要参数[1]			FSW-1	FSW-2
总质量[2]		kg	1 800～2 000	2 400
有效载荷[3]	可回收部分[4]	kg	150	300
	不可回收部分[5]	kg	150	400～500
轨道飞行时间[6]		d	5～8	10～15
近地点高度[7]		km	175～210	175～210
远地点高度[8]		km	300～400	300～400
周期[9]		min	90	90
轨道倾角[10]		(°)	57～70	57～70
微重力量级[11]		g_0	10^{-3}～10^{-5}	10^{-3}～10^{-5}

Key: 1. Main parameters; 2. Total mass; 3. Payload; 4. Recovered portion; 5. Unrecovered portion; 6. Time of orbital flight; 7. Altitude of perigee; 8. Altitude of apogee; 9. Period; 10. Dip angle in orbit; 11. Value of micro-gravity.

The paper was received for publication on 24 October 1990.

DERIVING RECOVERY MOTION EQUATIONS OF SATELLITE WITH QUATERNION RULE

Zhang Jian, of Beijing Institute of Spacecraft Systems Engineering

Abstract: Euler angles are used to describe angular motion and expressions for transforming from one coordinate system to another coordinate system, but there are problems with indeterminate solutions in the angular-motion equations described by this method. During satellite reentry, the attitude angles vary over a wide range and sometimes it is difficult to avoid singularities. By adopting a quaternion rule, the singularity problem can be fundamentally resolved, thus effectively upgrading the computational accuracy and speed. On this basis, the paper presents equations for satellite reentry motion.

Key words: Equation of motion, computational method, reentry orbit, recovery satellite.

I. Foreword

Generally, the Euler angle method is adopted in describing the equations for converting from one coordinate system to another and for describing angular motion. As is well known, there is always the problem of indeterminate solutions in the angular-motion equations described by the Euler angle method. In usage, generally speaking the variation range of angles is controlled so that there is no crossing of singularities. During

satellite reentry, especially for an uncontrolled ballistic reentry body, the variation range of its angles is quite large; sometimes, it is very difficult to avoid singularities. This gives rise to many difficulties in orbital design and computation; the computational accuracy is not easily controlled.

By using the quaternion rule, this singularity problem can be basically resolved; this approach can also effectively improve computational speed and accuracy.

There are two major shortcomings with the quaternion rule: one shortcoming is that it is not as simple and direct as in the Euler angle description method; the other shortcoming is the fact that the four elements describing angular motion are not independent. Due to the existence of the error of integration, the longer integration period may lead to divergence of the equation. Therefore, it is required to be based on accuracy requirements in selecting an appropriate revision method. This paper will not present in detail the quaternion revision problem; descriptions are available in related papers. The paper explains only briefly how to adopt the quaternion rule to derive the return motion equations.

II. Angular Motion Described by the Quaternion Rule

A. Quaternion

The quaternion is a number composed of a real number 1 and three imaginary numbers i, j, and k, with the following form:

$$E=\rho+\lambda i+\mu j+\nu k \qquad (1)$$

In the equation, ρ, λ, μ, ν are four components of the quaternion; they are all real numbers.

The summation of the square of the quaternion components is a constant,

$$\rho^2+\lambda^2+\mu^2+\nu^2=a= \text{ constant} \qquad (2)$$

When constant a is equal to 1, this quaternion is called the standard quaternion, that is,

$$\rho^2+\lambda^2+\mu^2+\nu^2=1 \qquad (3)$$

B. Terminal rotation

In Fig. 1, Oxyz is the fixed-coordinate system; $Ox_1y_1z_1$ is a traveling coordinate system bound to a rigid body; $\vec{n}$ is the instantaneous rotating axis line, bound to $Ox_1y_1z_1$. $\vec{B}$ is collinear with the rotating axis $\vec{n}$. Its mode is

$$|\vec{B}| = 2\operatorname{tg}\frac{\Phi_r}{2} \tag{4}$$

In the equation, Φ_r is the angle of rotation.

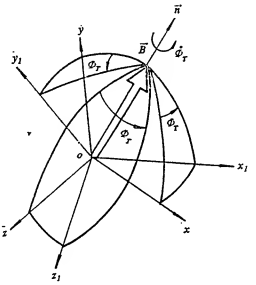

Fig. 1. Vector of terminal rotation

Vector $\vec{B}$ is called the vector of terminal rotation; the corresponding revolution is called the terminal rotation.

Eq. (4) is written in a component form:

$$\vec{B} = \begin{pmatrix} b_x \\ b_y \\ b_z \end{pmatrix} = \begin{pmatrix} 2\operatorname{tg}\frac{\Phi_r}{2}n_x \\ 2\operatorname{tg}\frac{\Phi_r}{2}n_y \\ 2\operatorname{tg}\frac{\Phi_r}{2}n_z \end{pmatrix} \tag{5}$$

In the equation, n_x, n_y, n_z are the three directional cosines of $\vec{B}$ (see Fig. 1).

By taking real numbers:

$$\left.\begin{aligned} \rho &= \cos\frac{\Phi_r}{2} \\ \lambda &= \frac{1}{2}\rho b_x = \sin\frac{\Phi_r}{2} n_x \\ \mu &= \frac{1}{2}\rho b_y = \sin\frac{\Phi_r}{2} n_y \\ \nu &= \frac{1}{2}\rho b_z = \sin\frac{\Phi_r}{2} n_z \end{aligned}\right\} \tag{6}$$

Then we have, $\rho^2+\lambda^2+\mu^2+\nu^2=1$; that is, ρ, λ, μ, ν can be considered as the four quaternion components, generally called the Rodrigues-Hamilton parameters.

Eq. (6) is the fundamental form of the quaternion describing angular displacement; Eq. (6) is of equal order with Eq. (5).

C. Using the Rodrigues-Hamilton parameters to express the matrix of directional cosines.

Referring to Fig. 1, transform from coordinate system Oxyz to $Ox_1y_1z_1$. The transformed matrix expressed by directional cosines is:

$$L = \begin{pmatrix} \cos\langle x_1,x\rangle & \cos\langle y_1,x\rangle & \cos\langle z_1,x\rangle \\ \cos\langle x_1,y\rangle & \cos\langle y_1,y\rangle & \cos\langle z_1,y\rangle \\ \cos\langle x_1,z\rangle & \cos\langle y_1,z\rangle & \cos\langle z_1,z\rangle \end{pmatrix} \tag{7}$$

In the equation, $\cos\langle i,j\rangle$, $(i=x_1,y_1,z_1;\ j=x,y,z)$, indicate the cosines of the angles included between the two coordinate axes. However, what matrix L actually is, is the directional cosine matrix transformed from $Ox_1y_1z_1$ to Oxyz; in other words,

$$\begin{pmatrix} x \\ y \\ z \end{pmatrix} = L \begin{pmatrix} x_1 \\ y_1 \\ z_1 \end{pmatrix} \tag{8}$$

But not

$$\begin{pmatrix} x_1 \\ y_1 \\ z_1 \end{pmatrix} = L \begin{pmatrix} x \\ y \\ z \end{pmatrix}$$

As presented in the paper, all cosine matrices are based on the above-mentioned derivation; this is mainly from the authors' habit, considering that this approach is more convenient to the projection of force (refer to Eqs. (29) and (30)), and also the approach is convenient in using the synthetic rotation formula (refer to Eq. (16)). Under ordinary situations, the expression for the equation of the directional cosine matrix L of synthetic rotation for n-th continuous rotation is:

$$L = L_n \cdot L_{n-1} \cdot \cdots\cdots \cdot L_2 \cdot L_1 \tag{9}$$

However, if $L_1, L_2, \cdots, L_n$ according to the derivation by means of Eq. (7); in other words, this indicates that the rotational sequence just the reverse. The first revolution is L_n; the n-th rotation is L_1. Therefore the synthetic rotation L should be

$$L = L_1 \cdot L_2 \cdot \cdots\cdots \cdot L_n \tag{10}$$

By using the directional cosines n_x, n_y, n_z of terminal rotation vector $\vec{B}$, as well as the angle of rotation Φ_T to express Eq. (7), a brief explanation is given as follows:

In Fig. 2 Φ_x, Φ_y and Φ_z represent the included angle between $\vec{n}$ and x, y, and z axes; in other words,

$$\left.\begin{aligned} \cos\Phi_x &= n_x \\ \cos\Phi_y &= n_y \\ \cos\Phi_z &= n_z \end{aligned}\right\} \tag{11}$$

$\langle x_1, x\rangle$, $\langle x_1, y\rangle$ and $\langle x_1, z\rangle$ indicate, respectively, the included angle between the x_1 axis and the x, y, and z axes.

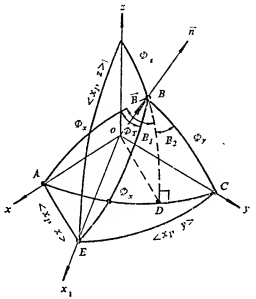

Fig. 2. Geometric relationships

From the triangle ABE on the spherical surface we can easily obtain

$$\cos\langle x_1, x\rangle = \cos\Phi_x\cos\Phi_z + \sin\Phi_x \cdot \sin\Phi_z\cos\Phi_\tau$$

From Eq. (11), we can easily obtain

$$\cos\langle x_1, x\rangle = n_x^2 + (1-n_x^2)\cos\Phi_\tau \tag{12}$$

From right triangle ABD on the spherical surface, we can obtain

$$\cos B_1 = \operatorname{ctg}\Phi_x \operatorname{tg}(90^\circ - \Phi_x) = \frac{\cos\Phi_x}{\sin\Phi_x}\,\frac{\cos\Phi_x}{\sin\Phi_x} = \frac{n_x n_z}{\sqrt{(1-n_x^2)(1-n_z^2)}}$$

$$\sin B_1 = \sqrt{1-\cos^2 B_1} = \frac{n_x}{\sqrt{(1-n_x^2)(1-n_z^2)}}$$

Similarly, from triangle CBD we obtain

$$\cos B_2 = \operatorname{ctg}\Phi_y \operatorname{tg}(90^\circ - \Phi_z) = \frac{n_y n_z}{\sqrt{(1-n_y^2)(1-n_z^2)}}$$

$$\sin B_2 = \frac{n_y}{\sqrt{(1-n_y^2)(1-n_z^2)}}$$

Therefore,

$$\cos B = \cos(B_1 + B_2) = \cos B_1 \cos B_2 - \sin B_1 \sin B_2$$

$$= -\frac{n_x n_y}{\sqrt{(1-n_x^2)(1-n_y^2)}}$$

$$\sin B = \sqrt{1-\cos^2 B} = -\frac{n_z}{\sqrt{(1-n_x^2)(1-n_y^2)}}$$

Therefore, from triangle BEC we obtain

$$\begin{aligned}\cos\langle x_1, y\rangle &= \cos\Phi_x \cos\Phi_y + \sin\Phi_x \cdot \sin\Phi_y \cos(B-\Phi_T) \\ &= n_x n_y (1-\cos\Phi_T) + n_z \sin\Phi_T\end{aligned} \tag{13}$$

By using a similar method, we can obtain all $\cos(i,j)$, $(i=x_1, y_1, z_1;\ j=x,y,z)$ in Eq. (7). Then we obtain the expression for the directional cosine matrix L expressed by directional cosines n_x, n_y, n_z and the rotational angle Φ_T of the terminal rotation vector $\vec{B}$ as:

$$L = \begin{pmatrix} n_x^2 + (1-n_x^2)\cos\Phi_T & n_x n_y (1-\cos\Phi_T) - n_z \sin\Phi_T \\ n_x n_y (1-\cos\Phi_T) + n_z \sin\Phi_T & n_y^2 + (1-n_y^2)\cos\Phi_T \\ n_x n_z (1-\cos\Phi_T) - n_y \sin\Phi_T & n_y n_z (1-\cos\Phi_T) + n_x \sin\Phi_T \\ n_x n_z (1-\cos\Phi_T) + n_y \sin\Phi_T & \\ n_y n_z (1-\cos\Phi_T) - n_x \sin\Phi_T & \\ n_z^2 + (1-n_z^2)\cos\Phi_T & \end{pmatrix} \tag{14}$$

By using Eq. (6) again with appropriate manipulation, we obtain the directional cosine matrix expressed by the Rodrigues-Hamilton parameter ρ, λ, μ and ν.

$$L = \begin{pmatrix} \rho^2+\lambda^2-\mu^2-\nu^2 & 2(-\rho\nu+\lambda\mu) & 2(\rho\mu+\lambda\nu) \\ 2(\rho\nu+\lambda\mu) & \rho^2+\mu^2-\lambda^2-\nu^2 & 2(\mu\nu-\rho\lambda) \\ 2(-\rho\mu+\lambda\nu) & 2(\rho\lambda+\mu\nu) & \rho^2+\nu^2-\mu^2-\lambda^2 \end{pmatrix} \tag{15}$$

D. Rodrigues-Hamilton parameter of synthetic rotation.

Assume ρ_1, λ_1, μ_1, ν_1 are the Rodrigues-Hamilton parameters of the first revolution; L_1 is the transformation matrix;

$\rho_2, \lambda_2, \mu_2, \nu_2$ are the Rodrigues-Hamilton parameters of the second revolution; L_2 is the transformation matrix;

ρ, λ, μ, ν are the Rodrigues-Hamilton parameters of two synthetic rotations; L is the synthetic transformation matrix;

Then we utilize

$$L=L_1 \cdot L_2 \tag{16}$$

After appropriate completion of the squares, finally we can derive the synthetic parameters:

$$\left.\begin{aligned}\rho&=\rho_1\rho_2-\lambda_1\lambda_2-\mu_1\mu_2-\nu_1\nu_2\\ \lambda&=\lambda_1\rho_2+\rho_1\lambda_2-\nu_1\mu_2+\mu_1\nu_2\\ \mu&=\mu_1\rho_2+\rho_1\mu_2-\lambda_1\nu_2+\nu_1\lambda_2\\ \nu&=\nu_1\rho_2+\rho_1\nu_2-\mu_1\lambda_2+\lambda_1\mu_2\end{aligned}\right\} \tag{17}$$

E. Equation of angular motion expressed by Rodrigues-Hamilton angular parameters.

Assume that $\omega_{x_1}, \omega_{y_1}, \omega_{z_1}$ are the three components of angular velocity $\dot{\varphi}_\tau \vec{n^0}$ on the three axes of the bound coordinate system $Ox_1y_1z_1$, then

$$\dot{\varphi}_\tau \vec{n^0}=\begin{pmatrix}\omega_{x_1}\\ \omega_{y_1}\\ \omega_{z_1}\end{pmatrix}$$

or

$$\left.\begin{aligned}\omega_{x_1}&=\dot{\varphi}_\tau n_x\\ \omega_{y_1}&=\dot{\varphi}_\tau n_y\\ \omega_{z_1}&=\dot{\varphi}_\tau n_z\end{aligned}\right\} \tag{18}$$

In the equation, $\vec{n^0}$ indicates the unit vector on the $\vec{n}$ axis.

With the derivation of Eq. (6), and taking note of Eq. (18) for the distribution of terms, we can obtain the following symmetric, linear angular motion equations:

$$\left.\begin{aligned}
\dot{\rho} &= -\frac{1}{2}(\omega_{x_1}\lambda+\omega_{y_1}\mu+\omega_{z_1}\nu)\\
\dot{\lambda} &= \frac{1}{2}(\omega_{x_1}\rho-\omega_{y_1}\nu+\omega_{z_1}\mu)\\
\dot{\mu} &= \frac{1}{2}(\omega_{x_1}\nu+\omega_{y_1}\rho-\omega_{z_1}\lambda)\\
\dot{\nu} &= \frac{1}{2}(-\omega_{x_1}\mu+\omega_{y_1}\lambda+\omega_{z_1}\rho)
\end{aligned}\right\} \tag{19}$$

Manipulate the above equations into the expression ω_{x_1}, ω_{y_1}, ω_{z_1} and then we have

$$\left.\begin{aligned}
\omega_{x_1} &= 2(-\lambda\dot{\rho}+\rho\dot{\lambda}+\nu\dot{\mu}-\mu\dot{\nu})\\
\omega_{y_1} &= 2(-\mu\dot{\rho}-\nu\dot{\lambda}+\rho\dot{\mu}+\lambda\dot{\nu})\\
\omega_{z_1} &= 2(-\nu\dot{\rho}+\mu\dot{\lambda}-\lambda\dot{\mu}+\rho\dot{\nu})
\end{aligned}\right\} \tag{20}$$

F. Relation between Rodrigues-Hamilton parameters and Euler angle

The rotation in Fig. 1 is indicated by the Euler angle; refer to Fig. 3.

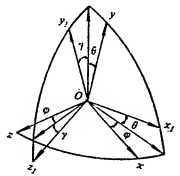

Fig. 3. Selection of Euler angle

From the approach of selecting the Euler angle in Fig. 3 we can easily obtain the Rodrigues-Hamilton parameters in three rotations expressed in terms of Euler angles:

$$
\left.
\begin{aligned}
\rho_1 &= \cos\frac{\varphi}{2} \\
\lambda_1 &= 0 \\
\mu_1 &= \sin\frac{\varphi}{2} \\
\nu_1 &= 0
\end{aligned}
\right\}
\left.
\begin{aligned}
\rho_2 &= \cos\frac{\theta}{2} \\
\lambda_2 &= 0 \\
\mu_2 &= 0 \\
\nu_2 &= \sin\frac{\theta}{2}
\end{aligned}
\right\}
\left.
\begin{aligned}
\rho_3 &= \cos\frac{\gamma}{2} \\
\lambda_3 &= \sin\frac{\gamma}{2} \\
\mu_3 &= 0 \\
\nu_3 &= 0
\end{aligned}
\right\}
$$

By using the synthetic rotation formulas Eqs. (10) and (17), we can easily derive the relation between the Rodrigues-Hamilton parameters and Euler angles:

$$
\left.
\begin{aligned}
\rho &= \cos\frac{\varphi}{2}\cos\frac{\theta}{2}\cos\frac{\gamma}{2} - \sin\frac{\varphi}{2}\sin\frac{\theta}{2}\sin\frac{\gamma}{2} \\
\lambda &= \cos\frac{\varphi}{2}\cos\frac{\theta}{2}\sin\frac{\gamma}{2} + \sin\frac{\varphi}{2}\sin\frac{\theta}{2}\cos\frac{\gamma}{2} \\
\mu &= \sin\frac{\varphi}{2}\cos\frac{\theta}{2}\cos\frac{\gamma}{2} + \cos\frac{\varphi}{2}\sin\frac{\theta}{2}\sin\frac{\gamma}{2} \\
\nu &= \cos\frac{\varphi}{2}\sin\frac{\theta}{2}\cos\frac{\gamma}{2} - \sin\frac{\varphi}{2}\cos\frac{\theta}{2}\sin\frac{\gamma}{2}
\end{aligned}
\right\} \qquad (21)
$$

Expressed in terms of Euler angles, the transformation matrix (15) is

$$
L = \begin{pmatrix}
\cos\varphi\cos\theta & -\cos\varphi\sin\theta\cos\gamma + \sin\varphi\sin\gamma & \cos\varphi\sin\theta\sin\gamma + \sin\varphi\cos\gamma \\
\sin\theta & \cos\theta\cos\gamma & -\cos\theta\sin\gamma \\
-\sin\varphi\cos\theta & \sin\varphi\sin\theta\cos\gamma + \cos\varphi\sin\gamma & -\sin\varphi\sin\theta\sin\gamma + \cos\varphi\cos\gamma
\end{pmatrix} \qquad (22)
$$

By comparing the corresponding terms in Eq. (21) and (15), we can easily obtain the equation showing the relation between the Euler angles and the Rodrigues-Hamilton parameters:

$$\sin\theta = 2(\rho\nu + \lambda\mu)$$
$$\operatorname{tg}\gamma = \frac{2(\rho\lambda - \mu\nu)}{\rho^2 + \mu^2 - \nu^2 - \lambda^2} \qquad (23)$$
$$\operatorname{tg}\varphi = \frac{2(\rho\mu - \lambda\nu)}{\rho^2 + \lambda^2 - \mu^2 - \nu^2}$$

III. Deriving equations for return motion

A. Coordinate system and transformation matrix

Generally, the three following coordinate systems are used in satellite return motion:

(1) Topocentric coordinate system Oxyz: this coordinate system is used as the datum to determine satellite position and attitude. The origin of coordinates is at the intersection of satellite diametral direction and the ellipsoid surface of the earth. The Oy axis is the diametral direction from satellite to the earth's surface; the Ox axis points to the direction of the initial path, perpendicular to the Oy axis. The Oz axis (together with Ox and Oy) forms a right-handed orthogonal coordinate system.

(2) Missile body-bound coordinate system $O_1x_1y_1z_1$: this coordinate system is used to determine satellite attitude. Generally, the origin of coordinates is the center of mass; the O_1x_1 axis is coincident with the longitudinal axis line of the satellite, pointing to its nose cone. The O_1y_1 axis is perpendicular to the O_1x_1 axis, generally located within the longitudinal plane of symmetry of the satellite. Together with the O_1x_1 and the O_1y_1 axes, the O_1z_1 axis forms a right-handed orthogonal coordinate system.

(3) Velocity coordinate system $O_1x_cy_cz_c$: this coordinate system is used to determine the velocity direction of the satellite mass center. The origin coincides with the origin of the missile body-bound coordinate system; the O_1x_c axis is aligned with the velocity direction. The O_1y_c axis is

perpendicular to the O_1x_c axis, located within the satellite's longitudinal symmetric surface. The O_1z_c axis, together with the O_1x_c and the O_1y_c axes forms a right-handed orthogonal coordinate system.

Let ρ_1, λ_1, μ_1, ν_1 be the Rodrigues-Hamilton parameters of Oxyz corresponding to $O_1x_1y_1z_1$; from Eq. (15), the transformation matrix is

$$L_1=\begin{pmatrix} A_{11} & B_{11} & C_{11} \\ A_{12} & B_{12} & C_{12} \\ A_{13} & B_{13} & C_{13} \end{pmatrix} = \begin{pmatrix} \rho_1^2+\lambda_1^2-\mu_1^2-\nu_1^2 & 2(-\rho_1\nu_1+\lambda_1\mu_1) & 2(\rho_1\mu_1+\lambda_1\nu_1) \\ 2(\rho_1\nu_1+\lambda_1\mu_1) & \rho_1^2+\mu_1^2-\lambda_1^2-\nu_1^2 & 2(\mu_1\nu_1-\rho_1\lambda_1) \\ 2(-\rho_1\mu_1+\lambda_1\nu_1) & 2(\rho_1\lambda_1+\mu_1\nu_1) & \rho_1^2+\nu_1^2-\mu_1^2-\lambda_1^2 \end{pmatrix} \tag{24}$$

ρ_2, λ_2, μ_2, ν_2 are the Rodrigues-Hamilton parameters of Oxyz corresponding to $O_1x_cy_cz_c$ from Eq. (15), the transformation matrix

$$L_2=\begin{pmatrix} A_{21} & B_{21} & C_{21} \\ A_{22} & B_{22} & C_{22} \\ A_{23} & B_{23} & C_{23} \end{pmatrix} = \begin{pmatrix} \rho_2^2+\lambda_2^2-\mu_2^2-\nu_2^2 & 2(-\rho_2\nu_2+\lambda_2\mu_2) & 2(\rho_2\mu_2+\lambda_2\nu_2) \\ 2(\rho_2\nu_2+\lambda_2\mu_2) & \rho_2^2+\mu_2^2-\lambda_2^2-\nu_2^2 & 2(\mu_2\nu_2-\rho_2\lambda_2) \\ 2(-\rho_2\mu_2+\lambda_2\nu_2) & 2(\rho_2\lambda_2+\mu_2\nu_2) & \rho_2^2+\nu_2^2-\mu_2^2-\lambda_2^2 \end{pmatrix} \tag{25}$$

ρ_3, λ_3, μ_3, ν_3 are the Rodrigues-Hamilton parameters of $O_1x_cy_cz_c$ corresponding to $O_1x_1y_1z_1$; from Eq. (15), the transformation matrix

$$L_3=\begin{pmatrix} A_{31} & B_{31} & C_{31} \\ A_{32} & B_{32} & C_{32} \\ A_{33} & B_{33} & C_{33} \end{pmatrix} = \begin{pmatrix} \rho_3^2+\lambda_3^2-\mu_3^2-\nu_3^2 & 2(-\rho_3\nu_3+\lambda_3\mu_3) & 2(\rho_3\mu_3+\lambda_3\nu_3) \\ 2(\rho_3\nu_3+\lambda_3\mu_3) & \rho_3^2+\mu_3^2-\lambda_3^2-\nu_3^2 & 2(\mu_3\nu_3-\rho_3\lambda_3) \\ 2(-\rho_3\mu_3+\lambda_3\nu_3) & 2(\rho_3\lambda_3+\mu_3\nu_3) & \rho_3^2+\nu_3^2-\mu_3^2-\lambda_3^2 \end{pmatrix} \tag{26}$$

In the equation, ρ_1, λ_1, μ_1 and ν_1 are used to determine

the satellite attitude, as obtained from integration of angular dynamics equation (40) (see text below). ρ_2, λ_2, μ_2 and ν_2 are used to determine the velocity orientation; these quantities can be obtained from relation Eq. (46). However, ρ_3, λ_3, μ_3 and ν_3 are determined by the revolution relations ① and ② (refer to Fig. 4).

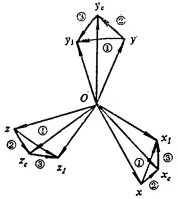

Fig. 4. Revolution relation between coordinate systems

From the definition of the Rodrigues-Hamilton parameters of the various coordinate systems mentioned above, Fig. 4 shows the revolution relations among three coordinate systems determined by the dynamic equations from practical applications. In other words, revolution ① of $O_1x_1y_1z_1$ can be considered as the synthetic revolution of $O_1x_cy_cz_c$ corresponding to revolution ② of Oxyz, and $O_1x_1y_1z_1$ corresponding to revolution ③ of $O_1x_cy_cz_c$. Then, from Eq. (16) we obtain

$$\left.\begin{aligned}\rho_1&=\rho_2\rho_3-\lambda_2\lambda_3-\mu_2\mu_3-\nu_2\nu_3\\ \lambda_1&=\lambda_2\rho_3+\rho_2\lambda_3-\nu_2\mu_3+\mu_2\nu_3\\ \mu_1&=\mu_2\rho_3+\nu_2\lambda_3+\rho_2\mu_3-\lambda_2\nu_3\\ \nu_1&=\nu_2\rho_3-\mu_2\lambda_3+\lambda_2\mu_3+\rho_2\nu_3\end{aligned}\right\} \qquad (27)$$

From Eq. (27) we obtain λ_3, μ_3 and ν_3.

Multiply ρ_1、λ_1、μ_1、ν_1, respectively, by ρ_2、λ_2、μ_2、ν_2 to be substituted in Eq. (27); we then obtain

$$\rho_3=\rho_2\rho_1+\lambda_2\lambda_1+\mu_2\mu_1+\nu_2\nu_1$$

By using a similar method, we obtain λ_3, μ_3 and ν_3 in sequence. As a result,

$$\left.\begin{aligned}\rho_3&=\rho_2\rho_1+\lambda_2\lambda_1+\mu_2\mu_1+\nu_2\nu_1\\ \lambda_3&=-\lambda_2\rho_1+\rho_2\lambda_1+\nu_2\mu_1-\mu_2\nu_1\\ \mu_3&=-\mu_2\rho_1-\nu_2\lambda_1+\rho_2\mu_1+\lambda_2\nu_1\\ \nu_3&=-\nu_2\rho_1+\mu_2\lambda_1-\lambda_2\mu_1+\rho_2\nu_1\end{aligned}\right\} \tag{28}$$

B. Equations for expressing projection of force and moment

(1) Thrust $\vec{P}$

Generally, an orbit-changing engine (braking rocket) serves to cause the satellite leave its operating orbit to enter the return orbit. Generally, the direction of $\vec{P}'$ is consistent with the O_1x_1 axis of the bound coordinate system of the satellite (missile body). From the transformation matrix Eq. (24), we can obtain the projection equation $\vec{P}$ in the topocentric coordinates system Oxyz,

$$\begin{pmatrix}P_x\\P_y\\P_z\end{pmatrix}=L_1\begin{pmatrix}P_{x_1}\\P_{y_1}\\P_{z_1}\end{pmatrix} \tag{29}$$

In Eq. (29), in standard state situations, thrust $\vec{P}$ points in the Ox_1 direction, the principal axis of the missile body. Then Px_1 is equivalent to scalar P of $\vec{P}$. Py_1, Pz_1 are equal to zero. With the deflection situation of thrust,
are components of the Ox_1, Oy_1, and Oz_1 axes.

(2) Gasdynamic force and gasdynamic moment

Let R_x, R_y, R_z stand the projection of gasdynamic force $\vec{R}$ on the topocentric coordinate system; x, y, z are the projections of the gasdynamic force $\vec{R}$ on the velocity coordinate system. Then from transformation matrix (25), we obtain

$$\begin{pmatrix}R_x\\R_y\\R_z\end{pmatrix}=L_2\begin{pmatrix}x\\y\\z\end{pmatrix} \tag{30}$$

In the equation,

$$x=-\frac{1}{2}\rho_m V^2 S C_D$$
$$y=\frac{1}{2}\rho_m V^2 S C_{yc} \qquad (31)$$
$$z=\frac{1}{2}\rho_m V^2 S C_{zc}$$

In the equations, ρ_m is atmospheric density; V is velocity; S is reference area; C_D is the resistance parameter along the Ox_c direction of the velocity coordinate system $Ox_cy_cz_c$; C_{yc} is the lift coefficient along the direction Oy_c. C_{zc} is the lateral-force coefficient along the direction Oz_c.

C_D, C_{yc}, and C_{zc} are determined by the axial-force coefficient and the normal-force coefficient; however, C_x and C_n are generally functions of the angle of attack, Mach number, and altitude. Fig. 5 shows the relation among the coefficients.

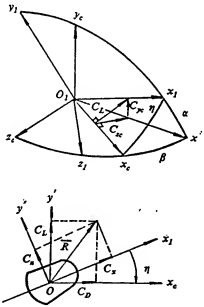

Fig. 5. Projection relations among gasdynamic-force coefficients

In Fig. 5, α is angle of attack; β is sideslip angle; and η is the total angle of attack. These parameters are determined by the following equation:

$$\cos\eta=\cos\alpha\cos\beta \qquad (32)$$

In Fig. 5, C_D is the resistance coefficient; C_L is called the (total) lift force coefficient.

From Fig. 5, we can obtain the following relation equations:

$$\left.\begin{aligned} C_{zc} &= \frac{-\cos\alpha\sin\beta}{\sin\eta}C_L \\ C_{yc} &= \frac{\sin\alpha}{\sin\eta}C_L \end{aligned}\right\} \tag{33}$$

$$\left.\begin{aligned} C_D &= C_x\cos\eta + C_n\sin\eta \\ C_L &= C_n\cos\eta - C_x\sin\eta \end{aligned}\right\} \tag{34}$$

To obtain α, β, and η, the directional cosine matrix (transformation matrix) can be derived by using the Euler angles (α and β):

$$L_3 = \begin{pmatrix} \cos\alpha\cos\beta & -\sin\alpha\cos\beta & \sin\beta \\ \sin\alpha & \cos\alpha & 0 \\ -\cos\alpha\sin\beta & \sin\alpha\sin\beta & \cos\beta \end{pmatrix} \tag{35}$$

By comparing Eqs. (26) and (35) we can easily obtain

$$\left.\begin{aligned} \sin\alpha &= 2(\rho_3\nu_3 + \lambda_3\mu_3) = A_{32} \\ \cos\alpha &= \rho_3^2 + \mu_3^2 - \lambda_3^2 - \nu_3^2 = B_{32} \end{aligned}\right\} \tag{36}$$

$$\left.\begin{aligned} \sin\beta &= 2(\rho_3\mu_3 + \lambda_3\nu_3) = C_{31} \\ \cos\beta &= \rho_3^2 + \nu_3^2 - \mu_3^2 - \lambda_3^2 = C_{33} \end{aligned}\right\} \tag{37}$$

From Eq. (32) and the two above-mentioned equations, we obtain

$$\cos\eta = (\rho_3^2 + \mu_3^2 - \lambda_3^2 - \nu_3^2)(\rho_3^2 + \nu_3^2 - \mu_3^2 - \lambda_3^2) = B_{32}\cdot C_{33} \tag{38}$$

The equations expressing gasdynamic moments M_{y1} and M_{z1} are similar to the method of projecting gasdynamic force. Then we can easily obtain

$$\left.\begin{aligned} M_{y_1} &= m_{z_1} q S l \frac{\sin\beta}{\sin\eta} \\ M_{z_1} &= m_{z_1} q S l \frac{\sin\alpha\cos\beta}{\sin\eta} \end{aligned}\right\} \tag{39}$$

In the equation, m_{z1} is the sideslip motion coefficient; this coefficient is a function of parameters (angle of attack, Mach number, and altitude); $q = \frac{1}{2}\rho_m V^2$ is the velocity head.

3. Derivation of Rodrigues-Hamilton parameters of missile body-bound coordinate system

The Rodrigues-Hamilton parameters of the missile body-bound coordinate system $O_1x_1y_1z_1$ are obtained by integrating the following angular motion equations. From Eq. (19), we can write out these motion equations:

$$\left.\begin{aligned}\dot{\rho}_1&=-\frac{1}{2}(\omega_{x_1}\lambda_1+\omega_{y_1}\mu_1+\omega_{z_1}\nu_1)\\ \dot{\lambda}_1&=\frac{1}{2}(\omega_{x_1}\rho_1-\omega_{y_1}\nu_1+\omega_{z_1}\mu_1)\\ \dot{\mu}_1&=\frac{1}{2}(\omega_{x_1}\nu_1+\omega_{y_1}\rho_1-\omega_{z_1}\lambda_1)\\ \dot{\nu}_1&=\frac{1}{2}(-\omega_{x_1}\mu_1+\omega_{y_1}\lambda_1+\omega_{z_1}\rho_1)\end{aligned}\right\} \tag{40}$$

We should note here that from Eq. (6) we know that

$$\rho_1^2+\mu_1^2+\lambda_1^2+\nu_1^2=1 \tag{41}$$

When integrating Eq. (40), condition (41) cannot be satisfied because of the existence of an integration error; when the error accumulates to a certain extent, the equation will be divergent. Therefore, when necessary, we should consider a revision of Eq. (40). In this paper we will not discuss in more detail the problem of revising the quaternion, as there are quite a few descriptions in the literature.

D. Derivation of Rodrigues-Hamilton parameters of velocity coordinate system

From the three components V_x, V_y, V_z of known velocity V on the topocentric coordinate system Oxyz, we can obtain the ballistic dip angle θ and the ballistic deflection angle ψ_c (refer to Fig. 6).

$$\sin\theta=\frac{V_y}{V},\quad |\theta|\leqslant\frac{\pi}{2} \tag{42}$$

$$\left.\begin{aligned}\sin\phi_c&=-\frac{V_z}{V\cos\theta}\\ \cos\phi_c&=\frac{V_x}{V\cos\theta}\end{aligned}\right\} \tag{43}$$

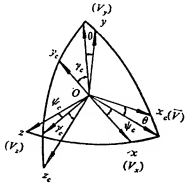

Fig. 6. Euler angle revolution of velocity coordinate system

From Fig. 6, the roll angle γ_c is constrained; refer to Fig. 5. The O_1y_c axis is constrained within the plane $O_1x_1y_1$ (within the longitudinal plane of the satellite). This constraint condition can be obtained by first projecting the O_1y_c axis onto Oxyz, and then projecting onto $O_1x_1y_1z_1$. In other words, this satisfies

$$C_{11}B_{21}+C_{12}B_{22}+C_{13}B_{23}=0 \tag{44}$$

Substitute B_{21}, B_{22}, and B_{23} into, respectively, indicating the directional cosines. In other words,

$$B_{21}=-\cos\phi_c\sin\theta\cos\gamma_c+\sin\phi_c\sin\gamma_c$$
$$B_{22}=\cos\theta\cos\gamma_c$$
$$B_{23}=\sin\phi_c\sin\theta\cos\gamma_c+\cos\phi_c\sin\gamma_c$$

After manipulation, the equation expressing γ_c is obtained

$$\operatorname{tg}\gamma_c=\frac{A_{23}(C_{11}A_{22}-C_{12}A_{21})+A_{23}(C_{13}A_{22}-C_{12}A_{23})}{C_{13}A_{21}-C_{11}A_{23}} \tag{45}$$

By using Eq. (21), the Rodrigues-Hamilton parameters of the velocity coordinate system can be written out:

$$\left.\begin{aligned}
\rho_2 &= \cos\frac{\psi_e}{2}\cos\frac{\theta}{2}\cos\frac{\gamma_e}{2} - \sin\frac{\psi_e}{2}\sin\frac{\theta}{2}\sin\frac{\gamma_e}{2} \\
\lambda_2 &= \cos\frac{\psi_e}{2}\cos\frac{\theta}{2}\sin\frac{\gamma_e}{2} + \sin\frac{\psi_e}{2}\sin\frac{\theta}{2}\cos\frac{\gamma_e}{2} \\
\mu_2 &= \sin\frac{\psi_e}{2}\cos\frac{\theta}{2}\cos\frac{\gamma_e}{2} + \cos\frac{\psi_e}{2}\sin\frac{\theta}{2}\sin\frac{\gamma_e}{2} \\
\nu_2 &= \cos\frac{\psi_e}{2}\sin\frac{\theta}{2}\cos\frac{\gamma_e}{2} - \sin\frac{\psi_e}{2}\cos\frac{\theta}{2}\sin\frac{\gamma_e}{2}
\end{aligned}\right\} \tag{46}$$

E. Return motion equations

All problems relating to deriving the motion equations and the quaternion have been solved as mentioned in the foregoing text. For completeness, general forms of the motion equations are listed without detailed explanations.

The mass-center motion equations:

$$\left.\begin{aligned}
m\frac{dV_x}{dt} &= P_x + R_x + W_{kcx} + mg_x \\
m\frac{dV_y}{dt} &= P_y + R_y + W_{kcy} + mg_y \\
m\frac{dV_z}{dt} &= P_z + R_z + W_{kcz} + mg_z
\end{aligned}\right\} \tag{47}$$

In the equations, W_{kcx}, W_{kcy}, W_{kcz} are representative terms of the Coriolis force and the drag force, selected as required. The items containing g are gravitational items.

Angular-motion equations:

$$\left.\begin{aligned}
\frac{d\omega_{x_1}}{dt} &= \frac{1}{D}(D_{11}W_{x_1} + D_{12}W_{y_1} + D_{13}W_{z_1}) \\
\frac{d\omega_{y_1}}{dt} &= \frac{1}{D}(D_{21}W_{x_1} + D_{22}W_{y_1} + D_{23}W_{z_1}) \\
\frac{d\omega_{z_1}}{dt} &= \frac{1}{D}(D_{31}W_{x_1} + D_{32}W_{y_1} + D_{33}W_{z_1})
\end{aligned}\right\} \tag{48}$$

In the equations, D and D_{ij} are the coefficients of inertial properties.

$$\left.\begin{aligned}
W_{x_1} &= \sum_i M_{ix1} + M_{x1} + \omega_{x_1}H_{y_1} - \omega_{y_1}H_{z_1} \\
W_{y_1} &= \sum_i M_{iy1} + M_{y1} + \omega_{z_1}H_{z_1} - \omega_{z_1}H_{z_1} \\
W_{z_1} &= \sum_i M_{iz1} + M_{z1} + \omega_{y_1}H_{z_1} - \omega_{z_1}H_{y_1}
\end{aligned}\right\} \tag{49}$$

In the equations, $\sum_i M_{i,1}, \sum_i M_{i,1}, \sum_i M_{i,1}$ are the terms of the gasdynamic damping moment and perturbation moment;

M_{X1} is the terms of axial-direction gasdynamic moment, which is unrelated to coordinate transformation, therefore there was no mention of it in the foregoing text. H_{x_1}, H_{y_1}, H_{z_1} are the components of the momentum torque.

The paper was received for publication on 8 July 1990.

DIGITAL ATTITUDE CONTROL SYSTEM AND FLIGHT TEST RESULTS OF CHINA'S RETURNABLE SATELLITES

Chen Yiqing, Chen Zugui, Sun Chengqi, Wang Xudong, Feng Yueyi, and Ding Guangcheng, all of Beijing Institute of Control Engineering

Abstract: The paper briefly presents schemes of the computer digital attitude control system used in China's returnable satellites. Design methods of attitude determination and phase plane control logic are described. Lastly, the results of flight tests are briefly described.

Key words: Digital control system, attitude control, spaceborne computer, systems engineering.

EXPLANATION OF SYMBOLS

oxyz is the satellite-bound coordinate system. The system coincides with the orbital coordinate system when there is no attitude deviation. In this case, oz points to the earth's center; oy points to the negative normal direction of the orbital plane; and ox points to the flight direction. These are called, respectively, the yaw axis, pitch axis, and roll axis.

ϕ、θ、ψ represent, respectively, the angles of roll, pitch, and yaw; $\hat{\phi}$、$\hat{\theta}$、$\hat{\psi}$ are the estimated values of ϕ、θ、ψ .

d_ϕ、d_θ、d_ψ are the related portions of indicators of gyroscopic drift; $\hat{d}_\phi$、$\hat{d}_\theta$、$\hat{d}_\psi$ are the estimated values of d_ϕ、d_θ、d_ψ .

b_ϕ、b_θ、b_ψ are the gyroscope constant drift.

$\hat{b}_\phi$、$\hat{b}_\theta$、$\hat{b}_\psi$ are their estimated values.

$\triangle\phi_H$ is the constant-value error of the roll infrared earth sensor; $\triangle\hat{\phi}_H$ is the estimated value of $\triangle\phi_H$.

ϕ_H and θ_H are, respectively, the outputs from the roll infrared earth sensor, and the pitch infrared earth sensor.

S_{ox}、S_{oy}、S_{oz} are the projection components on the coordinate axis of the orbital coordinate system of a unit vector $\vec{S}$ along the line connecting the satellite to the sun; S_{bx}、S_{by} and S_{bz} are the projection components of $\vec{S}$ on the coordinate axes of the satellite coordinate system.

α_ϕ and α_ψ are, respectively, the outputs of two single-axis sun trackers.

a_d is the satellite angular acceleration induced by interference moment; $\hat{a}_d$ is its estimated value.

I. General Description

The digital attitude control system was developed based on work done in developing the attitude control system [1,2] with simulation in China's first-generation returnable satellites. The system has the following major missions: eliminate the satellite initial deviation when the carrier rocket separates from the satellite; during the orbital operation period, the system serves to satisfy the requirements on attitude and attitude angular rate demanded by directional earthward observations; the system serves to reveal the return attitude required by the satellite rotating about its pitch axis before returning to the ground. As to the performance of the digital attitude control system, the authors made the following obvious improvements:

(1) Upgrade the accuracy of attitude determination and attitude control, and enhance attitude stability.

(2) Along the yaw direction, yaw angle control is adopted. In other words, the satellite rotates by angle $\phi_y(t)$ about the yaw axis in order to eliminate the component of lateral-direction velocity related to satellite remote sensing instruments by

landmarks induced by the earth's rotation.

(3) Reduce fuel consumption in order to prolong satellite service life.

The execution mechanism of the digital attitude control system is the reaction gas jetting system. On various axes, the angular acceleration generated by small nozzles (small thrusts) is $0.1deg/s^2$. On the pitch axis, large nozzles capable of producing $0.5deg/s^2$ serve to accelerate the satellite rotation around the pitch axis. With respect to the roll and yaw axes, simultaneous operation of two nozzles can provide acceleration of $0.2deg/s^2$. For the pitch axis, simultaneous operation of one large and one small nozzle can provide large thrust acceleration of $0.6deg/s^2$.

The system applies two conical scanning infrared earth sensors to measure satellite pitch and roll angles. Two digital sun trackers with 128deg x 128deg visual field are adopted, mainly to upgrade the determination accuracy of the yaw attitude. Three single-degree-of-freedom liquid floating rate integrating gyroscopes are used to measure, respectively, the components w_x, w_y, w_z on the satellite-bound coordinate axes of the satellite angular rate.

The system has the following important characteristics: information processing capability is greatly increased because a spaceborne computer is used; in addition, flexibility of system design and of practical operation is increased in order to upgrade system performance. The initial yaw deviation is eliminated, and attitude control at the return attitude adjusting stage is executed. The computer computational period is 0.26s; it is 1.04s in the orbital operating stage. During this period, the computer completes the collection of data for attitude sensors, data processing, and the issuing of commands for the corresponding gas jetting pulses, if necessary.

Fig. 1 shows the principle of the overall digital attitude control system.

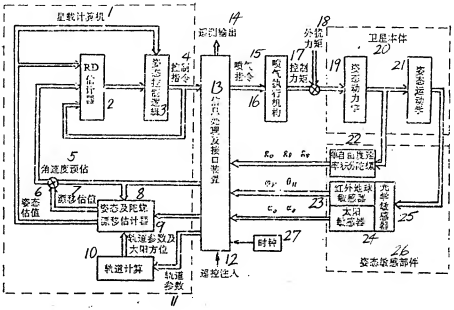

Fig. 1. Principle of attitude control system
KEY: 1 - Onboard satellite computer 2 - Estimating device 3 - Attitude control logic 4 - Control command 5 - Angular rate estimate 6 - Estimated attitude value 7 - Estimated drift value 8 - Attitude and gyroscope drift estimating device 9 - Orbital parameters and solar orientation 10 - Orbital computation 11 - Orbital parameters 12 - Input of remote control 13 - Information processing and interface installation 14 - Output of remote sensing 15 - Gas jetting command 16 - Gas jetting execution mechanism 17 - Control moment 18 - Perturbation moment 19 - Attitude dynamics 20 - Satellite body 21 - Attitude motion theory 22 - Single-degree-of-freedom velocity integrating gyroscope 23 - Infrared earth sensor 24 - Sun tracker 25 - Optical sensor 26 - Attitude sensing components 27 - Clock

II. System Design

Key points of design regarding the attitude determination algorithm, with a control computer, and attitude control law in the phase plane are described.

A. Attitude determination algorithm [3]

(1) Computation of satellite real-time orbit: Since the sun tracker is adopted in the digital attitude control system, it is necessary to conduct orbital computations of the satellite and the sun. Thus, the orientation (S_{ox}, S_{oy}, S_{oz}) of the sun in the orbital coordinate system is determined.

In computing the satellite orbit, an analytical method is applied [4]. One-order terms are usually taken for orbital gravity and atmospheric perturbation. The effect on flight-path error is greater owing to orbital decay; thus, second-order long-term perturbation terms are taken. In orbital computations, the angle of deviated current, $\phi_p(t)$, required for flight deviation, is also provided

$$\phi_p(t) = -\operatorname{arc\,tg}(V_n/V_t) \tag{1}$$

In the equation

$$V_n = \sqrt{\frac{\mu}{p}}(1+e\cos f) - \omega_e R_e \cos i \tag{2}$$

$$V_t = \omega_e R_e \sin i \sin u \tag{3}$$

With an uplink remote control channel, each day a ground station transmits once to the onboard satellite computer the measured orbital parameters and perturbation coefficient, thus continuously revising the parameters of the model for orbital dynamics, and ensuring the orbital computational accuracy in the satellite.

(2) Attitude estimating device: Attitude determination proceeds in two steps. In the first step, a new attitude estimate value is computed based on gyroscopic output and initial estimated attitude in a sampling period. The following computation formulas are adopted:

$$\left.\begin{aligned} \dot{\hat{\theta}} &= \omega_e - \hat{b}_\theta - \hat{d}_\theta + g_\theta \\ \dot{\hat{\phi}} &= \omega_e \hat{\psi} - \hat{b}_\phi - \hat{d}_\phi + g_\phi \\ \dot{\hat{\psi}} &= -\omega_e \hat{\phi} - \hat{b}_\psi - \hat{d}_\psi + g_\psi \end{aligned}\right\} \tag{4}$$

In the equation, g_θ, g_ϕ, g_ψ are the gyroscopic outputs.

Eliminate the state variation in phase plane controls of the

initial deviation stage and the return attitude adjustment stage; Eqs. (4) provide the attitude angle and attitude angular rate.

(3) Revision of attitude measurements: In the second step of attitude determination, based on the output of the optical attitude sensor in the same sampling period, the attitude estimate found by the estimating device is revised. The authors applied the well-known Kalman filtering method. The Kalman filter can execute comprehensive measurements and point out the state error, thus correctly revealing various useful information included in the measurements.

As the pitch channel is independent of the roll and yaw channels, therefore design can be separately conducted.

For the pitch channel, take the state vector as:

$$x_1=(\theta, d_\theta, b_\theta)^T$$

The state equation is

$$\dot{x}_1=A_1x_1+W_1+f_1$$

In the equation

$$A_1=\begin{pmatrix}0 & -1 & -1\\ 0 & -\beta_\theta & 0\\ 0 & 0 & 0\end{pmatrix},\quad W_1=\begin{pmatrix}W_\theta\\ W_{d\theta}\\ W_{b\theta}\end{pmatrix},\quad f_1=\begin{pmatrix}g_\theta\\ 0\\ 0\end{pmatrix} \qquad (5)$$

β_θ is the reciprocal of the time constant of the indicated drift of the pitch gyroscope; W_1 is the state noise.

The measurement equation is

$$z_1=H_1x_1+V_1 \qquad (6)$$

In the equation $H_1=(1,0,0)$; $z_1=\theta_m$; V_1 is the noise of the pitch infrared earth sensor.

From Eqs. (5) and (6), a stationary linear system Kalman filter can be constructed. Since the satellite operating time is very long, it can be designed for a stabilized filter; in other words, the estimate equation is

$$\dot{\hat{x}}_1=A_1x_1+f_1+K_m(z_1-H_1x_1) \qquad (7)$$

In the equation $K_m=(K_\theta, K_{d\theta}, K_{b\theta})^T$ is the steady-state increment matrix of Eqs. (5) and (6).

Since b_1 is the constant drift of the gyroscope, in theory $W_{b\theta}$ in Eq. (5) should be zero. However, in this way then

$K_{\delta\theta}=0$. Hence, here we should add virtual white noise $W_{\delta\theta}$ (such that its variance is nonzero). In actual applications, $K_{\delta\theta}=(1/3\sim1/6)K_{\delta\theta}$ in order to satisfy the time requirements on dynamic response.

The denominator of the transfer function in the closed-ring system (7) is

$$\Delta(s)=s^3+(K_\theta+\beta_\theta)s^2+(\beta_\theta K_\theta-K_{\delta\theta}-K_{\delta\theta})s-K_{\delta\theta}\beta_\theta \tag{8}$$

According to the performance of actually-measured components, various components of $K_{\pm}$ satisfy

$$K_\theta^2\gg-K_{\delta\theta}\gg-K_{\delta\theta}>0 \qquad -K_{\delta\theta}\gg\beta_\theta K_\theta>0 \tag{9}$$

Under conditions in which the above-mentioned relation is derived, three real roots of $\Delta(s)=0$ can be approximately obtained: $\lambda_1=-K_\theta$, $\lambda_2=K_{\delta\theta}/K_\theta$, $\lambda_3=-K_{\delta\theta}\beta_\theta/K_{\delta\theta}$.

$T_1=\frac{-1}{\lambda_1}$ is the responding time constant of Θ_H with respect to Θ;

$T_2=\frac{-1}{\lambda_2}$ is the responding time constant of ΘH with respect to d_θ and

$T_3=\frac{-1}{\lambda_3}$ is the responding time constant of ΘH with respect to b_θ .

For the roll-yaw channel, take the state vector as:

$$x_2=(\phi,\psi,d_\phi,d_\psi,b_\phi,b_\psi,\Delta\phi_H)^T$$

The state equation of the system is:

$$\dot{x}_2=A_2x_2+W_2+f_2 \tag{10}$$

in the equation

$$A_2=\begin{pmatrix} 0 & \omega_0 & -1 & 0 & -1 & 0 & 0 \\ -\omega_0 & 0 & 0 & -1 & 0 & -1 & 0 \\ 0 & 0 & -\beta_\phi & 0 & 0 & 0 & 0 \\ 0 & 0 & 0 & -\beta_\psi & 0 & 0 & 0 \\ 0 & 0 & 0 & 0 & 0 & 0 & 0 \\ 0 & 0 & 0 & 0 & 0 & 0 & 0 \end{pmatrix};\quad W_2=\begin{pmatrix} W_\phi \\ W_\psi \\ W_{d\phi} \\ W_{d\psi} \\ W_{b\phi} \\ W_{b\psi} \\ W\Delta\phi_H \end{pmatrix};\quad f_2=\begin{pmatrix} g_\phi \\ g_\psi \\ 0 \\ 0 \\ 0 \\ 0 \\ 0 \end{pmatrix} \tag{11}$$

The measurement vector is: $z_2=(\phi_H,\alpha_\phi,\alpha_\psi)^T$

The measurement equation is:

$$z_2=h(x_1,t)+V_2=\begin{pmatrix} \phi+\Delta\phi_H \\ \operatorname{arctg}(S_{By}/S_{Bx}) \\ \operatorname{arctg}S_{By}/[(S_{Bx}+S_{Bz})\sin 45^\circ] \end{pmatrix}+\begin{pmatrix} V_\phi \\ V_{w\phi} \\ V_{w\psi} \end{pmatrix} \tag{12}$$

In the equation, S_{Bx}、S_{By}、S_{Bz} are functions of S_{ox}、S_{oy}、S_{oz} and ϕ、ψ、θ .

State equation (11) is stationary-linear; however, measurement equation (12) is nonlinear and time-varying. Since ϕ、ψ、θ are small quantities, therefore $h(0,t)+H_2x_2$ can be used to approximate $h(x_2,t)$ to make it into a linear system.

$$H_2(t)=\frac{\partial h(x_2,t)}{\partial x_2}\Big|_{x_2=0} \tag{13}$$

From H_2, the system observability can be studied. In the sunlit zone, the system can be observed; in the shadow zone, the system state quantity $\Delta\phi_H$, d_ϕ, b_ϕ are unable to be observed. When $\beta_\phi\neq\beta_\psi$ although $d\phi$ can be observed, yet only weakly.

From the system made up of Eqs. (11) and (12), the estimate equation can be derived by using the Kalman filtering method:

$$\dot{\hat{x}}_2=A_2\hat{x}_2+f_2+K(t)[z_2-h(\hat{x}_2,t)] \tag{14}$$

A practical problem is that computation of K(t) is quite involved, as the capacity, speed, and wordlength of the onboard satellite computer cannot satisfy the requirements. Thus, a simplified method should be sought.

Noting that the measurement function $h(x_2,t)$, or $H_2(t)$ is a function of the period T (here T is the orbital period of the

satellite), therefore $H_2(t)$ is a measurement matrix of a periodically-varying coefficient. When t approaches infinity, K(t) approaches the increment matrix $K_\infty(t)$ of a stationary periodically-varying coefficient. Let us use a method for approximate simulation of a primitive function to $K_\infty(t)$, of period T to be stored in the internal memory of the onboard satellite computer. Thus, the computational volume and the storage capacity can be greatly reduced; in addition, the cumulative errors in computation can also be reduced.

In practical applications, the independent variable t in K(t) can be replaced by the periodic variables S_{xx}、S_{yy}、S_{zz}, ; $K(t)=K_\infty$ (S_{xx}, S_{yy}, S_{zz}) . In the shadow zone, the system dimensions are reduced; in other words, let $x_2=(\phi,\psi,d_\psi,b_\psi)^T$, $z_2=\phi_H$, , and let the stationary error-variance matrix P_∞ of the corresponding stationary linear system be used as the variance matrix P_0 of the system estimate error at the beginning of the sunlit zone, for computing the corresponding increment matrix. As revealed by practical simulation computations, it is simple and effective to use this method.

Consider that there is also error in orbital computation; this error should be revealed in z_2. The method involves the artificially increasing the corresponding noise $V_{s\phi}$ and $V_{s\psi}$; moreover, the variance of this noise is also time-varying (in other words they are also functions of S_{xx}、S_{yy}、S_{zz}). Thus, the measured noise has also a periodic time-varying property.

In designing, the effect of the pitch channel on the roll-yaw channel should be reduced (because z_2 is dependent on Θ). In other words, periodically increase the periodic components of $V_{s\phi}$ and $V_{s\psi}$.

(4) Estimate of attitude angular rate and perturbation angular rate: In the orbital operation stage, to reduce high-frequency noise in the angular rate signal, and to estimate the perturbation angular acceleration in order to raise the efficiency of gas jetting control, thus, the angular rate and

perturbation angular acceleration estimating device (briefly called the RD estimating device) is designed. To reduce error, the RD estimating device suspends its operation during the gas jetting periods. The three-axes RD estimating devices have the same form. Citing an example of the pitch axis, the state vector is $x_3=(\dot{\theta}, a_d)^T$. The state equation is

$$x_3=A_3x_3+W_3 \tag{15}$$

In the equation,

$$A_3=\begin{pmatrix}0 & 1\\ 0 & 0\end{pmatrix},\ W_3=\begin{pmatrix}0\\ W_d\end{pmatrix}.$$

W_d is virtual white noise with its nonzero variance, thus revealing the slow variation of acceleration with practical external perturbation (mainly gasdynamic perturbation). The automatic attitude estimating device, Eq. (4), is used for measurement z_3 of the RD estimating device, therefore the measurement equation is

$$z_3=H_3x_3+V_3 \tag{16}$$

In the equation, $H_3(1,0)$. V_3 is noise of the attitude estimating device. Therefore, we can obtain the result that the RD estimating device is

$$\hat{x}_3=A_3\hat{x}+K(z_3-H_3\hat{x}_3) \tag{17}$$

To select the increment coefficient K, it is determined from the requirements of two aspects: accuracy estimate and velocity-change estimate.

In the above-mentioned algorithms of attitude determination, the various continuous estimate equations are carried out with an appropriate divergence system in the onboard satellite computer.

B. Phase Plane Control Law [5]

In the different mission stages, different control laws are adopted. In the pitch mobile stage of eliminating the initial deviation and prior to satellite return, the "minimum fuel and time" is the performance indicator. During the orbital operation period, the performance indicator is "minimum error and gas jetting time".

The state variable of the phase plane is composed of the attitude estimate and the attitude angular rate estimate provided by the attitude determination algorithm. In the normal orbital operation period, in order to execute control of the deviated current angle, $\hat{\psi}-\psi_p$ is adopted as the angular deviation of the yaw phase plane for three-axes independent control. In addition to attitude mobility of pitch prior to satellite return, in other mission stages, basically the phase plane switching lines of various axes are the same. In the following, explanations are given by using pitch as the example.

Eliminate the phase plane switching line in the initial deviation stage and orbital operation stage, as shown in Fig. 2.

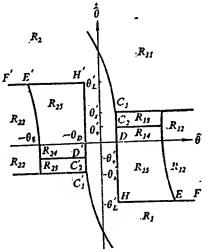

Fig. 2. Eliminate phase plane switching lines in the initial deviation phase and in the orbital stage

The entire phase plane is divided into several zones by switching lines; R_1 and R_2 are the closing zones. $R_{11}(R_{21})$ is the large-thrust all-open zone; $R_{12}(R_{22})$ and $R_{13}(R_{23})$ are the small-thrust all-open zones. In $R_{12}(R_{22})$, when the phase point approaches the closing line, HEF(H'E'F'), the duration of gas jetting should be determined by difference value computation of

this closing line. The value of $\dot{\theta}_L$ is scores of time greater in the stage of eliminating the initial deviation over the orbital operation stage. $R_{14}(R_{24})$ and $R_{15}(R_{25})$ are the small-thrust stepped zone; their main functions are:

1i. Execute the operation of limiting ring;

2i. Prevent the mistaken gas jetting due to an error in estimating the angular rate; and

3i. Prevent the continuous increase of attitude angle in $R_{15}(R_{25})$.

Concretely speaking, when the phase point enters $C_2D(C_2'D')$ from $R_{14}(R_{24})$ or when entering $DH(D'H')$ from $R_{15}(R_{25})$, gas jetting is immediately executed. In this zone, if the previous state is gas jetting, then a fixed value

$$Y=|\hat{\theta}_0|+\theta_v$$

is established. In the equation, $\hat{\theta}_0$ is the attitude estimate at the gas jetting time; θ_v is the fixed threshold value selected.

If the absolute value of the later attitude estimate is increased, the Y value remains unchanged. If the absolute value of the later attitude estimate is decreased, then the predetermined fixed value is changed into $Y=|\hat{\theta}|_{min}+\theta_v$. $|\hat{\theta}|_{min}$ is the minimum value of $|\hat{\theta}|$ in this period. The condition of the next gas jetting is $|\hat{\theta}|\geqslant Y_0$.

In $R_{14}(R_{24})$, the gas jetting duration is computed by using the following equation

$$T_M=T_{M1}+T_{M2} \tag{18}$$

In the equation

$$T_{M1}=|\hat{\dot{\theta}}|/a_2 \tag{19}$$

$$T_{M2}=\begin{cases}(K_1(|\hat{\theta}|-\theta_b')/a_2 & \text{eliminating initial deviation stage, pitch mobile stage, orbital stage (when } |\hat{a}_d|<a_{d*} \text{ or RD estimating device is not effective)} \\ \sqrt{2(|\hat{\theta}|+K_2\theta_D)|\hat{a}_d|+\delta}/a_2 & \text{orbital stage (when } |\hat{a}_d|\geqslant a_{d*}\text{)}\end{cases} \tag{20}$$

$$\delta=\begin{cases}1 & \operatorname{sign}\hat{\theta}=\operatorname{sign}\hat{\omega} \\ 0 & \operatorname{sign}\hat{\theta}=-\operatorname{sign}\hat{\omega}\end{cases} \tag{21}$$

Θ_D is the dead zone; its value is determined by the attitude control accuracy.

$\theta_0'=\theta_0-d_\theta$, d_θ、D_θ ; D_0 and K_1 are the preselected values; K_2 is a dimensionless factor smaller than 1.

The second equation of Eqs. (20) reveals that the gas jetting duration is moderated by the estimated value of external perturbation in order to execute single-side limiting cycle operation of a longer period. The gas jetting duration in the $R_{1s}(R_{2s})$ zone is a fixed small-quantity T; the upper boundary of T is determined by the requirement imposed on attitude angular rate; the lower boundary of T is determined by the minimum impulse (double-side limiting ring of the longest period formed in a state without perturbation) given by the execution mechanism. Selection of T and of the threshold value θ_s should match between the control effect and the revised rate of the attitude estimate.

In the orbital operation stage, the crude control mode (widening the dead zone) is adopted in the period without perturbation.

Figs. 3 and 4 are, respectively, the mathematical simulation phase plane of the eliminating-initial-deviation stage and the orbital-operation stage.

C. Reliability Considerations in Systems Design

Design reliability of the system includes two aspects, component level and system level. The onboard satellite computer adopts a two-machine fault-tolerant technique; the multi-protection approach is adopted in the software layout. Based on system performance data, the computer operation state is graded by using the previously specified grade evaluation standard; when it is necessary, two-machine switching is automatically executed. Switching determination is arranged for the attitude determination system. For example, by using remote control

switching, the conventional mode of a gyrocompass is used without adopting the sun tracker. In the information processing occurring in the control system, the amplitude-limiting approach is appropriately adopted; hard locking protection is adopted for important comments. To reduce acting times of the electromagnetic tubes, automatic rotation of small nozzles of two similar thrusts of the roll axis and the yaw axis is carried out. A good effect was achieved with these measures in actual flights.

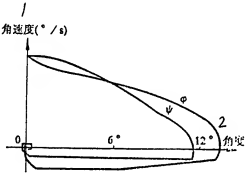

Fig. 3. Eliminating initial-deviation phase
KEY: 1 - Angular rate
2 - Angle

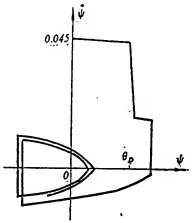

Fig. 4. Orbital operation yaw-axis phase (with function of perturbing moment)

III. Conclusions

In the digital attitude control system of China's returnable satellites, for the first time the single-degree-of-freedom rate integrating gyroscope and a highly precise digital sun tracker are adopted for the first time. By using modern control theory, system performance is improved. In flight tests, the satellite attitude control mission was successively accomplished. Based on the number of orbits provided by the ground, satellite orbital computation proceeds correctly. The sun tracker has the functions of marking the constant gyroscopic drift, and the error

in the constant value of the roll infrared earth sensor, thus enhancing accuracy in attitude determination. Prior to satellite return, large yaw-angle mobility is accomplished within a specified time period; thus, the satellite accurately returned to its predetermined touchdown point. By comparing with the simulation system prior to the improvements, the angular rate of orbital operation and gas consumption are apparently reduced; these show the gigantic development potential of the satellite control system after the onboard satellite computer is adopted.

The paper was received on 18 July 1990.

REFERENCES

1 Yang Jiachi, Zhang Guifu, Sun Chengqi. Three Axis Stabilization Attitude Control System for Chinese Near Earth Orbit Satellite. \[IFAC Symposium on Automatic Control in Space. Oxford, UK. 2—6. July 1979.

2. Yang Jiachi, Zhang Guofu, Sun Chengqi, Feng Hueyi, and Niu Yinsheng, "Attitude Control System and Flight Test Results of Returnable Earth Orientation Observation Satellite," YUHANG XUEBAO [Journal of Space Flight], No. 1, 1981

8 Compbell B H and Coffey T C. Digital Attitude Reference System (DARS). Navigation Journal of the Institute of Navigation, 1973, 20 (1).

4. Liu Lin, "Solution of Artificial Satellite Motion with Critical Orbital Dip Angle," TIANWEN XUEBAO [Journal of Astronomy], No. 15, 1974.

5 Cox K J. Case Study on Apollo lunar Module Digital Autopilot, Case Studies in System Control.

DISTRIBUTION LIST

DISTRIBUTION DIRECT TO RECIPIENT

ORGANIZATION	MICROFICHE
B085 DIA/RTS-2FI	1
C509 BALLOC509 BALLISTIC RES LAB	1
C510 R&T LABS/AVEADCOM	1
C513 ARRADCOM	1
C535 AVRADCOM/TSARCOM	1
C539 TRASANA	1
Q592 FSTC	4
Q619 MSIC REDSTONE	1
Q008 NTIC	1
Q043 AFMIC-IS	1
E051 HQ USAF/INET	1
E404 AEDC/DOF	1
E408 AFWL	1
E410 AFDTC/IN	1
E429 SD/IND	1
P005 DOE/ISA/DDI	1
P050 CIA/OCR/ADD/SD	2
1051 AFIT/LDE	1
P090 NSA/CDB	1
2206 FSL	1

Microfiche Nbr: FTD94C000551
NAIC-ID(RS)T-0651-94